Fine Chemical Engineering
https://ojs.wiserpub.com/index.php/FCE/

Research Article

Efficient Removal of Florasulam, Metalaxyl, and Thiamethoxam Pesticides from Water Using Carboxymethyl Cellulose-Functionalized Magnetic Graphene Oxide Nanoparticles

Mostafa A. I. Taha[1], Mohamed E. I. Badawy[1*], Reda K. Abdel-Razik[2], Mahmoud M. Abo-El-Saad[1]

[1]Department of Pesticide Chemistry and Technology, Faculty of Agriculture, Alexandria University, Alexandria, El-Shatby, 21545, Egypt
[2]Mammalian Toxicology Department, Central Agricultural Pesticide Laboratory, Agricultural Research Center, Alexandria, El-Sabahia, 21616, Egypt
E-mail: mohamed.badawy@alexu.edu.eg

Received: 29 July 2025; **Revised:** 16 September 2025; **Accepted:** 17 October 2025

Graphical Abstract:

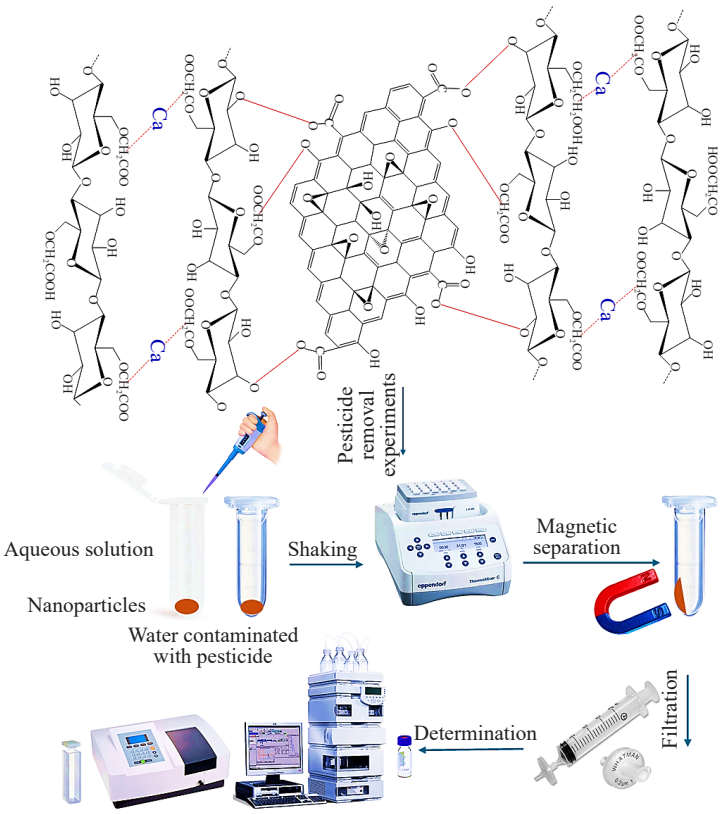

DOI: https://doi.org/10.37256/fce.7120268048

Abstract: Magnetic Graphene Oxide Nanoparticles (MGO-NPs) and a series of Carboxymethyl Cellulose-functionalized Magnetic Graphene Oxide Nanoparticles (CMC-MGO-NPs) were prepared for application as adsorbents in pesticide removal. Three distinct CMC-MGO-NPs were prepared by varying the weight ratios of CMC to MGO-NPs (1 : 1, 3 : 1, and 5 : 1, w/w). The nanocomposites were characterized using Scanning Electron Microscopy (SEM), Fourier Transform Infrared Spectroscopy (FTIR), and zeta potential analysis, which confirmed their successful preparation. In addition, specific surface area and porosity were determined. These products were then evaluated for their efficiency in removing florasulam, metalaxyl, and thiamethoxam pesticides from aqueous solutions. Key operational parameters were optimized using a Plackett-Burman factorial design, which identified pesticide concentration, adsorbent dosage, temperature, pH, agitation time, and ionic strength as the most statistically significant factors affecting removal efficiency. Significantly, the CMC-MGO-NPs-2 demonstrated high maximum removal efficiencies of 93.82% for florasulam and 88.10% for metalaxyl, highlighting their strong affinity for these pesticides. However, a lower efficiency of 28.46% was observed for thiamethoxam, indicating selectivity in the adsorption process. In addition, the adsorption of pesticides onto CMC-MGO-NPs-2 was evaluated using various kinetic and isotherm models. These results underscore the potential of CMC-MGO-NPs-2 as a highly effective, low-cost, and magnetically separable adsorbent for the remediation of specific pesticides from wastewater.

***Keywords*:** carboxymethyl cellulose-magnetic graphene oxide nanoparticles, pesticides, adsorption, High-Performance Liquid Chromatography (HPLC) analysis

1. Introduction

Global pesticide use has steadily increased over the past decades, led to a near doubling of global use between 1990 and 2018.[1,2] Integrated strategies like Integrated Pest Management (IPM) and Integrated Vector Management (IVM) are vital for reducing reliance on chemical pesticides. However, pesticides are still a necessary tool for food production and public health in many situations.[3] The persistence of pesticides in the environment is a major concern, as their slow degradation leads to long-term soil and water contamination. This persistence facilitates bioaccumulation, where these chemicals accumulate in organism tissues, and biomagnification, where their concentration increases in the food chain.[4] This poses significant risks to human health, including acute toxicity and chronic effects such as endocrine disruption and cancer. Furthermore, ecosystems are severely impacted by their toxicity to non-target organisms, including pollinators such as bees and aquatic organisms, disrupting biodiversity and ecological balance. In these cases, it's crucial to minimize the negative impacts on human health and the environment. The global database of pesticide applications has enabled the modeling of global environmental contamination risks for 92 pesticides across 168 countries.[5] The extensive use of pesticides like florasulam (herbicide), metalaxyl (fungicide), and thiamethoxam (insecticide) in Egypt raises concerns about pesticide residues contaminating drinking water and groundwater.[6,7] These pesticides pose various environmental and health risks. Florasulam can persist in the soil and leach into groundwater, potentially harming sensitive aquatic plants and disrupting aquatic ecosystems.[8] Metalaxyl is highly soluble and mobile, posing a similar risk to water pollution. Although its human toxicity is low, it can cause eye and skin irritation.[9] Thiamethoxam is a neonicotinoid insecticide associated with significant harm to pollinators such as bees, contributing to colony collapse disorder. It is also suspected of having toxic effects on human growth and reproduction.[10] The widespread use of these pesticides underscores the risk of bioaccumulation and ecological imbalance on a broader scale.

Several techniques are used to remove pesticides from water systems, including adsorption, membrane technology, biological remediation, and electrochemical remediation.[11] Of these methods, adsorption is the simplest to operate and has the lowest operation and maintenance costs. Additionally, this method offers the advantage of regenerating and recycling the adsorbent, and it rarely produces secondary pollutants.[12] While well-known and cost-effective, adsorption's effectiveness for water treatment depends on several factors. These include the adsorbent's capacity, permeability, surface area, and its affinity for the specific contaminant being targeted. Despite this variation, adsorption has proven highly successful in removing a range of harmful pollutants from water.[11]

Various studies are investigating biodegradable and eco-friendly composite materials for various environmental applications.[13,14] Among these materials, Carboxymethyl Cellulose (CMC) stands out as a natural, abundant, effective,

and low-cost biopolymer.[15] Beyond its uses in food, pharmaceuticals, and other industries, CMC is a promising adsorbent for removing toxic contaminants including pesticides. This potential stems from CMC's unique chemical structure which the presence of carboxyl and hydroxyl groups allows it to interact with pollutants through various mechanisms. The abundant hydroxyl groups on the glucopyranose rings can form hydrogen bonds with contaminants.[16] In addition, the overall surface area of CMC facilitates adsorption through chelation.[17]

Graphene Oxide (GO), a promising nanomaterial, is just one atom thick and made from carbon atoms in a honeycomb pattern. This unique structure gives it special properties like a large network of freely moving electrons.[18] GO takes this a step further by adding oxygen-containing groups like carboxylic acids, epoxides, and hydroxyls to the graphene oxide's surface. These groups make GO strongly attracted to water (hydrophilic) and give it an exceptional ability to adsorb pollutants.[19] Magnetic GO Nanoparticles (MGO-NPs) are known for their tiny size and ease of manipulation with magnets. This allows for easy separation of MGO-NPs from water after it has captured pollutants, simplifying the purification process.[20]

Combining MGO-NPs with CMC creates a material (CMC-MGO-NPs) with a higher capacity to adsorb pollutants.[12] This is because CMC-MGO-NPs have a rougher surface area compared to MGO-NPs.[21] The increased surface area allows for more beneficial functional groups to be present, which further improves adsorption.[22] Because of this, CMC-MGO-NPs are a promising material for removing pollutants like pesticides, heavy metals, and azo dyes from water.[12]

This study presents a simple and economical approach for removing pesticides from water. The method utilizes CMC-MGO-NPs synthesized through a co-precipitation technique. These composites act as adsorbents, capturing pesticide molecules from the aqueous environment. Therefore, Fe_3O_4 magnetic particles were prepared and dispersed on GO surface, then reacted it into the CMC composite to form CMC-MGO-NPs. The chemical and physical properties were examined using various techniques like Scanning Electron Microscopy (SEM), zeta potential, and Fourier Transform Infrared Spectroscopy (FTIR). In addition, specific surface area and porosity determinations were determined. A special design (factorial Plackett-Burman design) helped to optimize the pesticide removal processes and know the effect of critical operating parameters. Key adsorption parameters, such as pesticide concentration, adsorbent dosage, temperature, pH, agitation time, and ionic strength, were optimized to enhance removal efficiency. Moreover, pesticide adsorption on CMC-MGO-NPs was analyzed with various kinetic and isotherm models. To our knowledge, the novelty of this work is the development of a "green", magnetically separable, highly selective nanocomposite (CMC-MGO-NPs), whose use for the removal of pesticides of different chemical groups was optimized using a sophisticated statistical approach, revealing important insights into the mechanisms of selective adsorption. This represents an advance in the field of applied environmental nanotechnology, providing a practical, effective, and sustainable solution for targeted wastewater treatment.

2. Materials and methods

2.1 *Pesticides and chemicals*

High-purity pesticides technical grade, florasulam (96%), metalaxyl (97%), and thiamethoxam (96%), were supplied by Shoura Chemicals Co. (Egypt). Graphite powder and Carboxymethyl Cellulose (CMC) were obtained from Sigma-Aldrich (USA), while High-Performance Liquid Chromatography (HPLC)-grade solvents (acetonitrile, methanol, and water) were purchased from Merck (Germany). A 0.2 μm Polyvinyl Difluoride (PVDF) syringe filter (Whatman, USA) was used for filtration. All other chemicals, including hydrochloric acid, sulfuric acid, phosphoric acid, potassium permanganate (≥ 99%), hydrogen peroxide (30%), ferrous chloride ($FeCl_2 \cdot 4H_2O$, 98%), ferric chloride ($FeCl_3 \cdot 6H_2O$, 99%), calcium chloride ($CaCl_2$, 99%), sodium hydroxide (NaOH, 99%), and ammonium hydroxide (NH_4OH, ≥ 99%), were acquired from El-Gomhouria Co. (Egypt) and used as received.

2.2 *Preparation of CMC-MGO-NPs*

Firstly, GO was synthesized using the modified Hummers' method[23] as shown in Figure 1. Magnetic Graphene Oxide Nanoparticles (MGO-NPs) were then prepared from this GO using a chemical co-precipitation method,[12] as

illustrated in Figure 2. Secondly, CMC-MGO-NPs were prepared using the co-precipitation method[12] (Figure 2). Three CMC-MGO-NP composites were prepared by varying the weight ratios of CMC to MGO-NPs as follows: CMC-MGO-NPs-1 (1 : 1, w/w), CMC-MGO-NPs-2 (3 : 1, w/w), and CMC-MGO-NPs-3 (5 : 1, w/w). First, MGO-NPs were dispersed in 100 mL of deionized water and sonicated (75 kHz, 9 pulses/sec) for 15 min, followed by magnetic stirring for 3 h. Separately, an aqueous CMC solution was prepared and mixed with the MGO-NPs suspension at the specified ratios under stirring at 70 °C. The hydrogel matrix was crosslinked via dropwise addition of 0.1 M $CaCl_2$ and subsequently incubated quiescently for 12 h at room temperature to facilitate complete ionic gelation, yielding a magnetically separable composite. The precipitate was collected using a magnet, washed with ethanol and deionized water, and dried at 80 °C for 60 h.

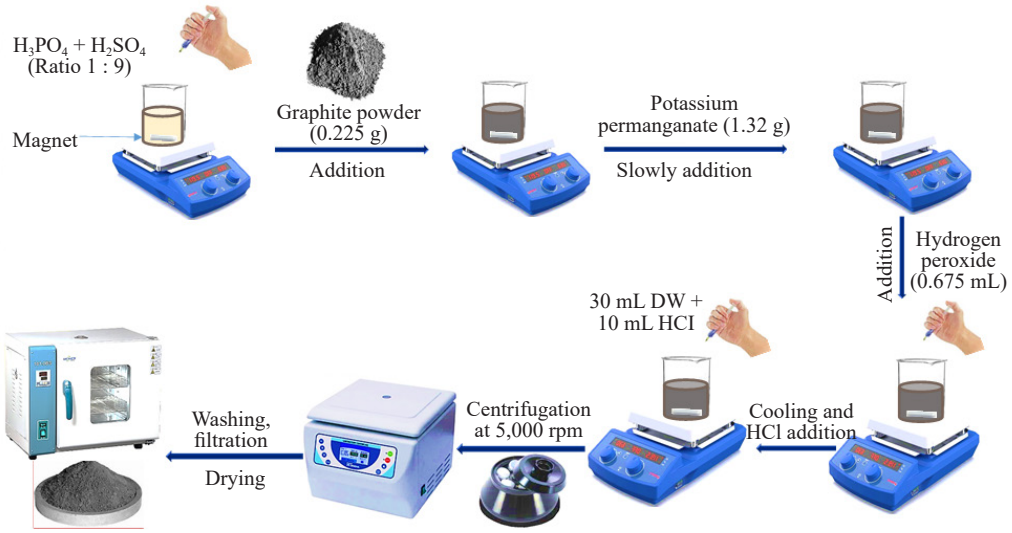

Figure 1. Schematized diagram of GO-NPs preparation

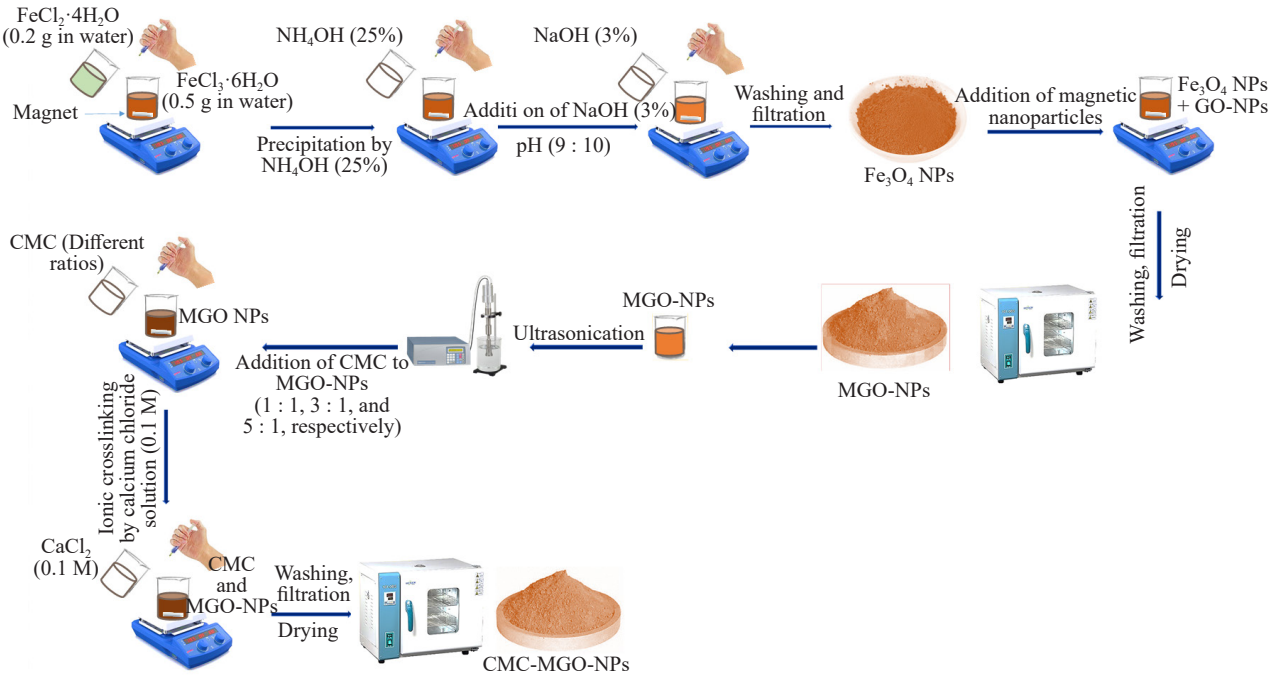

Figure 2. Schematized diagram of CMC-MGO-NPs preparation at ratios of 1 : 1, 3 : 1, and 5 : 1 for CMC and MGO-NPs, respectively

2.3 *Characterizations of MGO-NPs and CMC-MGO-NPs*

2.3.1 *SEM*

The morphology of the prepared nanoparticles was investigated using an SEM JEOL-JSM5300 microscope (Faculty of Science, Alexandria University, Alexandria, Egypt). Briefly, 0.01 gram of the product was suspended in alcohol and sonicated to prevent aggregation. After that, the nanoparticles were mounted to a metal stub with sticky tape (double-sided tape) and coated with a thin layer of gold. Finally, The nanoparticles were imaged with an accelerating potential of 20 kV.[24]

2.3.2 *Droplet size, polydispersity index, and zeta-potential*

The nanoparticle droplet size (nm) and Polydispersity Index (PDI) were measured at room temperature using a Zetasizer Nano ZS diffractometer (Malvern Instruments Ltd, UK) via Dynamic Light Scattering (DLS). To avoid multiple scattering effects, the particles were diluted in ultrapure water and sonicated for 5 minutes (9 cycles/sec, 5 kHz power) prior to analysis. The droplet's size was expressed as a mean diameter in nanometer.[25] In order to investigate the surface charge of the prepared nanoparticles based on the dynamic light scattering principal technique. A 0.01 g sample was dispersed in 10 mL of distilled water and sonicated for 15 min to achieve uniform suspension. Then, 2 mL of the dispersed sample were placed in a zeta-potential cell for analysis. Measurements were performed at 25 °C, neutral pH, and an applied voltage of 149 mV.

2.3.3 *Evaluating surface area and porosity*

Specific Surface Area (SSA, in m^2/kg) was analyzed with a Bettersizer 2600 laser diffraction particle size analyzer. Furthermore, material porosity (%) was determined by applying the void ratio method.[26] This approach first calculates the void ratio ($e = V_v/V_s$), which represents the proportion of void space to solid matter. Porosity (ϕ) is subsequently defined as the fraction of the total bulk volume ($V_b = V_v + V_s$) occupied by voids ($\phi = V_v/V_b$).

2.3.4 *FTIR spectroscopy*

The FTIR was performed to investigate the function group detections of nanoparticles by Perkin Elmer FTIR (Faculty of Pharmacy, Alexandria University, Alexandria, Egypt). The samples were individually mixed with KBr (1 : 20, w/w) and ground into a fine powder using an agate mortar. The Infrared (IR) spectra were obtained over the frequency range of 400 ~ 4,000 cm^{-1} at a resolution of 4.0 cm^{-1}.[27]

2.4 *Removal of pesticides by CMC-MGO-NPs*

2.4.1 *Optimization and design of experiment*

A preliminary experiment was conducted to investigate the effects of CMC-MGO-NPs-1, CMC-MGO-NPs-2, and CMC-MGO-NPs-3 on pesticide removal from water. Based on the results obtained, CMC-MGO-NPs-2 and CMC-MGO-NPs-3 were found to be comparable in removing the three pesticides compared to CMC-MGO-NPs-1. Due to their similar performance, CMC-MGO-NPs-2 was chosen for all subsequent experiments. A Design of Experiments (DOE) approach was applied to evaluate key factors, pesticide concentration, adsorbent dosage, temperature, pH, agitation time, and ionic strength, and their impact on the adsorption efficiency of florasulam, metalaxyl, and thiamethoxam by CMC-MGO-NPs-2. A 13-run full factorial design, including a center point, was implemented in MINITAB™ (v17.1.0) as shown in Table 1. Six variables were studied at three levels (coded -1, 0, and +1): pesticide concentration (25, 50, and 75 µg/mL), adsorbent amount (25, 50, and 75 mg), temperature (10, 25, and 40 °C), pH (5, 7, and 9), agitation time (10, 20, and 30 min), and ionic strength (0, 5, and 10% NaCl). Finally, the statistical analysis was conducted to identify which factors significantly affect the pesticide removal. This analysis will involve a polynomial equation ($Y = A_0 + A_1X_1 + A_2X_2 + A_3X_3 + A_nX_n$) that expresses the dependent variable (Y, removal %) as a function of independent factors (X_1 to X_n). In this equation, A_0 represents a constant value, while A_1 to A_n are the coefficients associated with each independent factor.[28]

Table 1. Full factorial experimental design matrix and analysis of factor effects on pesticide removal efficiency

Run order	Pesticide (µg/mL)	Adsorbent (mg)	Temperature (°C)	pH	Agitation (min)	Ionic strength (%)
1	+1 (75)	-1 (25)	+1 (40)	-1 (5)	-1 (10)	-1 (0)
2	+1 (75)	+1 (75)	-1 (10)	+1 (9)	-1 (10)	-1 (0)
3	-1 (25)	+1 (75)	+1 (40)	-1 (5)	+1 (30)	-1 (0)
4	+1 (75)	-1 (25)	+1 (40)	+1 (9)	-1 (10)	+1 (10)
5	+1 (75)	+1 (75)	-1 (10)	+1 (9)	+1 (30)	-1 (0)
6	+1 (75)	+1 (75)	+1 (40)	-1 (5)	+1 (30)	+1 (10)
7	-1 (25)	+1 (75)	+1 (40)	+1 (9)	-1 (10)	+1 (10)
8	-1 (25)	-1 (25)	+1 (40)	+1 (9)	+1 (30)	-1 (0)
9	-1 (25)	-1 (25)	-1 (10)	+1 (9)	+1 (30)	+1 (10)
10	+1 (75)	-1 (25)	-1 (10)	-1 (5)	+1 (30)	+1 (10)
11	-1 (25)	+1 (75)	-1 (10)	-1 (5)	-1 (10)	+1 (10)
12	-1 (25)	-1 (25)	-1 (10)	-1 (5)	-1 (10)	-1 (0)
13	0 (50)	0 (50)	0 (25)	0 (7)	0 (20)	0 (5)

The coded levels -1, 0, and +1 for each factor are the lowest value, center point, and highest value, respectively

2.4.2 *Removal of pesticides by CMC-MGO-NPs-2*

This experiment explored the use of nanoparticles to remove pesticides from water through adsorption. Aqueous solutions containing different pesticide concentrations (25, 50, and 75 µg/mL) were prepared, keeping the methanol content below 1% (v/v) to avoid cosolvent effects. Pesticide handling was conducted with appropriate personal protective equipment (gloves, goggles, and lab coat) within a fume hood. Individual pesticide aliquots were added to Eppendorf tubes containing nanoparticles, with a total volume of 2 mL. Handling of dry nanoparticles was performed in a fume hood to minimize inhalation risk. The experiment was conducted under different conditions. All experiments were performed in triplicate and the average values are reported. Afterward, a magnet was used to separate the pesticide-laden nanoparticles from the solution. The remaining liquid was passed through a special filter (0.22 µm Millipore syringe filter). This filtrate was analyzed by HPLC to determine pesticide removal efficiency.[27] The following equations were used to calculate the percentage of pesticide removal (Equation (1)), the adsorption capacity (q_e, Equation (2)), and the Enrichment Factor (EF, Equation (3)).

$$\text{Removal (\%)} = \left[\left(C_i - C_e\right)/C_i\right] \times 100 \quad (1)$$

$$q_e = \left[\left(C_i - C_e\right)/m\right] \times V \quad (2)$$

$$\text{EF} = C_e / C_i \quad (3)$$

Where, C_i: Initial concentration of the pesticide in the solution (µg/mL). C_e: Equilibrium concentration of the pesticide in the solution (µg/mL). m: Mass of the adsorbent (g). V: Volume of the solution (L).

2.5 *Kinetic and equilibrium analysis of adsorption processes*

2.5.1 *Kinetic behavior assessment*

The kinetic behavior of CMC-MGO-NPs-2 for the removal of the three pesticides was investigated using batch adsorption experiments. Working solution of a known initial concentration (C_0, 50 µg/mL) for each pesticide was prepared fresh by diluting the stock solution in deionized water, keeping the methanol content below 1% (v/v) to avoid cosolvent effects. All kinetic experiments were performed in 2 mL Eppendorf vials. For each experiment, a fixed dosage of CMC-MGO-NPs-2 adsorbent (50 mg) was added the pesticide solution 50 µg/mL at pH = 7. The mixture was immediately placed on an orbital shaker and agitated at a constant speed (150 rpm) at a controlled temperature (25 ± 1 °C). At predetermined time intervals (0, 5, 10, 15, 20, 25, and 30 min), the adsorbent was separated using a centrifuge at 5,000 rpm for 5 min or magnetically separated and filtered through a 0.22 µm Millipore syringe filter. The concentration of each pesticide in the supernatant (C_e, µg/mL) at each time point (t, min) was quantified using HPLC. All experiments were performed in triplicate, and the average values are reported. The amount of pesticide adsorbed onto CMC-MGO-NPs-2 at time t, q_t (mg/g), was calculated. The kinetic data (q_t vs. t) for each pesticide were fitted to several prevalent kinetic models to elucidate the adsorption mechanism and the rate-controlling steps. These models applied were: pseudo-first-order (4), pseudo-second-order (5), and intraparticle diffusion (6).

$$\log\left(q_e - q_t\right) = \log\left(q_e\right) - \left(K_1 / 2.303\right) \times t \tag{4}$$

Here, q_e denotes the equilibrium adsorption capacity (mg/g), q_t is the adsorption at time t (mg/g), K_1 represents the first-order rate constant (min^{-1}), and t is the contact time (min).

$$t / q_t = \left(1 / K_2 q_e^2\right) + \left(1 / q_e\right) \times t \tag{5}$$

Where K_2 is the second-order rate constant (g/mg·min), with other variables as defined previously. This framework often fits well with data involving chemical interactions between the adsorbent and adsorbate.

$$q_t = C_{id} + K_{id} t^{1/2} \tag{6}$$

In this equation, K_{id} is the intraparticle diffusion rate constant (mg/g·min), and C_{id} is an intercept reflecting boundary layer effects. A linear plot of q_t versus $t^{1/2}$ indicates if diffusion controls the process.

Finally, the linear and non-linear regression analysis for these models was performed. The goodness of fit for each model was evaluated and compared based on the correlation coefficient (R^2) and the percentage of the Sum of Squared Errors (% SSE).

2.5.2 *Equilibrium adsorption isotherms*

Batch adsorption experiments were conducted to determine the equilibrium adsorption isotherms of the three pesticides onto CMC-MGO-NPs-2. In a typical procedure, a fixed mass of CMC-MGO-NPs-2 (50 mg) was added to a series of 2 mL Eppendorf vials containing pesticide solution at varying initial concentrations (C_0; 10, 25, 50, 75, and 100 µg/mL) at pH = 7. The vials were then transferred to a temperature-controlled shaker incubator and agitated at a constant speed of (150 rpm) at 25 ± 1 °C for different periods (15, 20, and 25 min). After reaching equilibrium, the adsorbent was separated from the solution using an external magnet or centrifugation at 5,000 rpm. The supernatant was then carefully withdrawn and analyzed to determine the equilibrium concentration (C_e) of the pesticide by HPLC. All experiments were performed in triplicate, and the average values are reported. The amount of pesticide adsorbed at equilibrium (q_e, mg/g) was calculated. The experimental data points (q_e vs. C_e) for each pesticide were then fitted to classical adsorption isotherm models, namely the Freundlich (7), Langmuir (8), and Temkin (9) models, to analyze the adsorption capacity and mechanism.

$$\log(q_e) = \log(K_f) + 1/n(\log C_e) \quad (7)$$

K_f indicates the adsorption capacity (L/mg), $1/n$ is the adsorption intensity or surface heterogeneity, which indicates the energy distribution, q_e is the equilibrium uptake (mg/g), and C_e is the residual concentration (μg/L). This model excels for heterogeneous systems like natural adsorbents.

$$1/q_e = (1/bq_m C_e) + (1/q_m) \quad (8)$$

Here, q_m is the maximum monolayer capacity (mg/g), and b is the affinity constant (L/mg) linked to adsorption energy. It's ideal for scenarios with finite, equivalent binding sites.

$$q_e = (RT/b) \times \ln K_T + (RT/b) \times \ln C_e \quad (9)$$

K_T is the equilibrium binding constant (L/mol), b relates to the heat of adsorption (J/mol), R is the gas constant (kJ/mol·K), and T is absolute temperature (K). This approach is valuable for intermediate concentration ranges where heat variations are significant.

2.6 *HPLC analysis*

Stock solutions of florasulam, metalaxyl, and thiamethoxam (1 mg in 10 mL methanol) were prepared based on standard purity. Calibration curves were constructed using six concentration levels (0.0125-0.15 μg/mL) by plotting peak areas against standard concentrations for quantification in water samples. Pesticide residues were analyzed using an Agilent 1260 HPLC Infinity system (Germany) with a Ultraviolet (UV) detector, managed by HP Chemstation software. Detection wavelengths were set at 210 nm (florasulam), 220 nm (metalaxyl), and 254 nm (thiamethoxam). Separation was performed on a ZORBAX Eclipse Plus C_{18} column (250 × 4.6 mm, 5 μm) with a 5 μL injection volume. Florasulam was eluted at 1.61 ± 0.01 min using acetonitrile : methanol (70 : 30) at 1.3 mL/min. Metalaxyl eluted at 3.54 ± 0.01 min with acetonitrile : methanol : water (25 : 50 : 25) at 0.8 mL/min. Thiamethoxam eluted at 3.68 ± 0.01 min using acetonitrile : methanol (75 : 25) at 1 mL/min. Quantification was achieved by comparing sample peak areas to the standard calibration curves.[29]

2.7 *Statistical analysis*

Data are expressed as mean ± Standard Error (SE), with statistical significance defined at $p \leq 0.05$. A one-way Analysis of Variance (ANOVA) was performed, followed by post-hoc Student-Newman-Keuls (SNK) tests, using IBM SPSS Statistics 25.0 (SPSS Inc., Chicago, IL, USA).[30]

3. Results and discussion

3.1 *Preparation of MGO-NPs and CMC-MGO-NPs*

This study describes the preparation of GO nanostructures using a modified Hummer method.[23] The MGO-NPs were produced with a yield of 5.16 g and appeared brownish (Table 2). Similarly, CMC-MGO-NPs-1, CMC-MGO-NPs-2, and CMC-MGO-NPs-3 were prepared with yields of 1.14 g, 1.3 g, and 1.64 g, respectively. All CMC-MGO-NPs exhibited a light brown color. Graphite treated with a mixture of sulfuric acid, phosphoric acid, and potassium permanganate yields GO, which is rich in oxygen-containing functional groups such as carboxyl, hydroxyl, epoxy, and ketone. These hydrophilic groups enhance water dispersibility.[31] Additionally, GO's extensive network of π-electron systems grants it a high attraction for carbon-containing ring structures, commonly found in medications, pollutants, and biological molecules. Combining Fe_3O_4 nanoparticles with GO as a support material produces an MGO-NPs nanocomposite, offering a simple and efficient approach for Magnetic Solid Phase Extraction (MSPE).[32] This effectiveness stems from the negatively charged GO nanosheets attracting Fe^{3+} and Fe^{2+} ions in solution through van der

Waals forces and hydrogen bonds, allowing for high-density attachment.[33] In short, GO can interact with CMC chains through hydrogen bonding and van der Waals forces. These bonds form between the carboxylic groups on CMC and the hydroxyl groups on GO sheets.[34] Because of this good interaction and hydrogen bonding ability, GO can be easily dispersed through CMC microbeads, creating a network composite. Furthermore, the addition of calcium chloride ($CaCl_2$) as a crosslinking agent improves the stability of the CMC-MGO-NPs composite. The primary mechanism is ionic gelation (ionotropic gelation) facilitated by $CaCl_2$, rather than the formation of new covalent bonds. CMC is a polyanionic polymer with abundant -COO^- groups. $CaCl_2$ dissociates in water to provide Ca^{2+} ions. These divalent cations act as ionic crosslinkers, forming coordination complexes between the negatively charged carboxylate groups of adjacent CMC chains. This creates a three-dimensional hydrogel network, effectively trapping and embedding the MGO particles. This creates a robust composite matrix that can be separated using magnets.[35]

Table 2. Synthesis output and physiochemical properties for MGO-NPs and CMC-MGO-NPs

Product code	Reaction components	Product color	Weight before drying (g)	Weight after drying (g)	Particles diameter (nm) ± SE	PDI ± SE	Specific Surface Area (SSA, m^2/kg)	Porosity (%) ± SE
MGO-NPs	$FeCl_3$: $FeCl_2$: GO	Brown	6.71	5.16	62.09 ± 2.54	0.376 ± 0.06	2,032	39.24 ± 0.37
CMC-MGO-NPs-1	CMC : MGO : $CaCl_2$	Light brown	1.42	1.14	72.08 ± 1.68	0.445 ± 0.07	6,589	38.69 ± 0.44
CMC-MGO-NPs-2	CMC : MGO : $CaCl_2$	Light brown	1.76	1.31	93.41 ± 1.38	0.331 ± 0.05	5,149	34.12 ± 0.61
CMC-MGO-NPs-3	CMC : MGO : $CaCl_2$	Light brown	2.04	1.64	93.50 ± 1.78	0.453 ± 0.07	4,620	21.12 ± 0.79

MGO-NPs: Magnetic Graphene Oxide Nanoparticles, CMC-MGO-NPs-1: Carboxymethyl Cellulose Magnetic Graphene Oxide Nanoparticles (1 : 1, w/w), CMC-MGO-NPs-2: Carboxymethyl Cellulose Magnetic Graphene Oxide Nanoparticles (3 : 1, w/w), CMC-MGO-NPs-3: Carboxymethyl Cellulose Magnetic Graphene Oxide Nanoparticles (5 : 1, w/w), PDI: Polydispersity Index, and SE: Standard Error

3.2 *Characterizations of MGO-NPs and CMC-MGO-NPs*

3.2.1 *SEM*

The surface morphology of both MGO-NPs and CMC-MGO-NPs were examined using SEM. Figure 3 presents the obtained SEM images. As reported in the previous study,[12] the images show a layered structure with uneven shapes, like a flat sheet with rounded edges MGO-NPs and CMC-MGO-NPs. On the other hand, CMC-MGO-NPs exhibit a rough surface compared with MGO-NPs which shows that the composite formation of MGO with CMC resulted in a higher surface area.[12] While SEM is a powerful technique for visualizing the shape and size (morphology) of nanoparticles, its limitations often necessitate the use of complementary methods for comprehensive material characterization.

3.2.2 *Droplet size, PDI, and zeta-potential*

The average particle sizes increased as CMC content increased: 62.09 nm (MGO-NPs), 72.08 nm (CMC-MGO-NPs-1), 93.41 nm (CMC-MGO-NPs-2), and 93.50 nm (CMC-MGO-NPs-3) (Table 2). PDI values were 0.376, 0.445, 0.331, and 0.453 for the corresponding samples which indicates a more uniform particle size distribution and stability at pH = 7 and 25 °C. Literature suggests that a PDI between 0.05 and 0.7 reflects a well-dispersed sample with uniform droplet sizes (homogeneous system). In contrast, a PDI approaching 1 indicates a broad droplet size distribution, signifying a heterogeneous system.[36] The prepared nanoparticles exhibited negative surface charges. Figure 4a-d shows the zeta potential values of the nanoparticles. MGO-NPs had the highest negative value (-27.10 mV), followed by CMC-MGO-NPs-1 (-16.10 mV), CMC-MGO-NPs-2 (-2.60 mV), and CMC-MGO-NPs-3 (-0.15 mV). The zeta potential (ζ) is a crucial parameter that reflects the surface charge of nanoparticles in a suspension. It indicates the degree of electrostatic repulsion between the particles, which influences their stability in dispersion.[37] Negative zeta potential values are associated with a repulsion force between particles, contributing to their stability in suspension.[38]

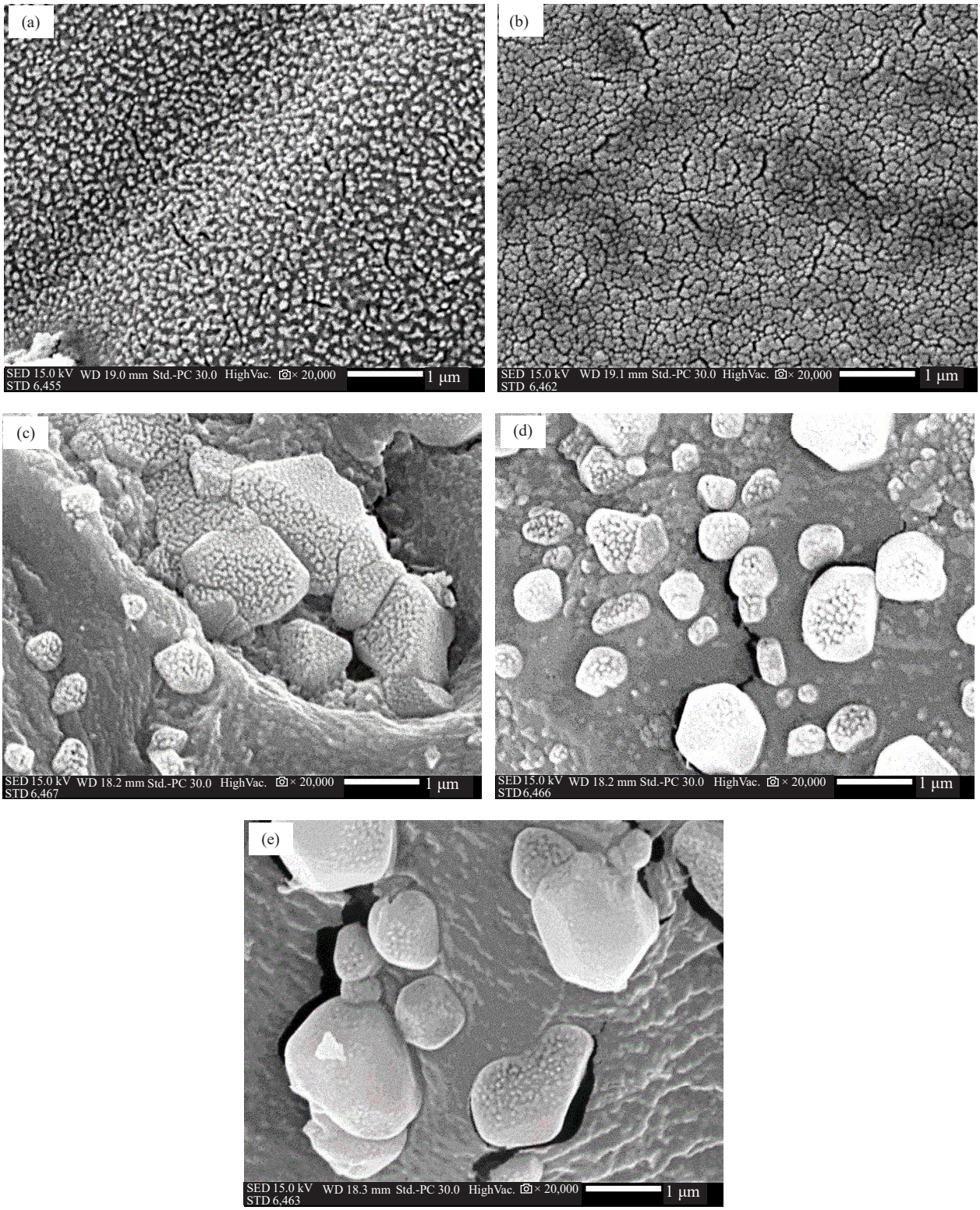

Figure 3. SEM of GO-NPs (a), MGO-NPs (b), CMC-MGO-NPs-1 (c), CMC-MGO-NPs-2 (d), and CMC-MGO-NPs-3 (e). The images of the particles were at scale bar 1 µm and magnification × 20,000 and 20 KV

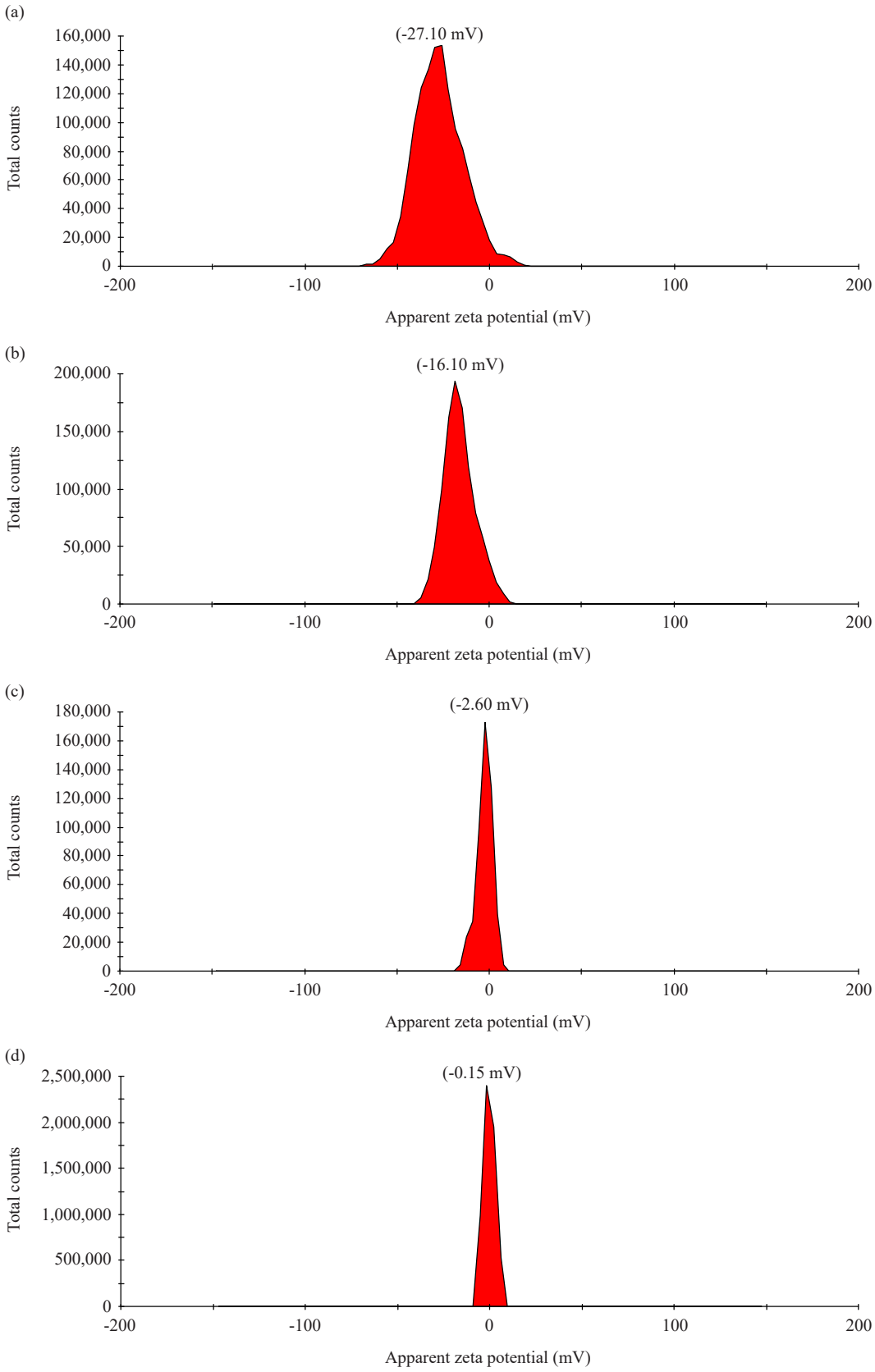

Figure 4. Zeta potential distribution graphs of MGO-NPs (a), CMC-MGO-NPs-1 (b), CMC-MGO-NPs-2 (c), and CMC-MGO-NPs-3 (d)

MGO-NPs tend to have a negatively charged surface because of oxygen-containing groups like carboxyl, epoxide, and hydroxyl groups clinging to their surface. These groups detach protons (H^+) when in water, leaving behind a negatively charged surface layer.[39] Anionic polymers, such as Polyvinylpyrrolidone (PVP) and CMC, can help MGO-NPs maintain this negative charge.[40,41] On the other hand, cationic polymers like Poly(diallyldimethylammonium chloride) (PDDA) and Chitosan (CS) can flip the surface charge to positive. The polymers attach to the MGO-NP surface via their positively charged amine groups, leading to a positive zeta potential.[42]

3.2.3 *The specific surface area and porosity*

The SSA and porosity of the synthesized nanoparticles are presented in Table 2. The SSA of MGO-NPs was 2,032 m^2/kg, which increased dramatically to 6,589 m^2/kg for the composite with the lowest CMC content (CMC-MGO-NPs-1). CMC-MGO-NPs-2, and CMC-MGO-NPs-3 showed 5,149, and 4,620 m^2/kg, respectively. However, both SSA and porosity exhibited a clear inverse relationship with CMC loading. For instance, porosity decreased from 39.24% for MGO-NPs to 21.12% for the composite with the highest CMC content (CMC-MGO-NPs-3). This trend is attributed to CMC integration forming cross-linked networks that occupy the interstitial spaces between MGO-NPs, thereby reducing the overall pore volume. Dolatabadi et al.[12] synthesized MGO-CMC for the remediation of chlorpyrifos-contaminated groundwater. Characterization of the adsorbent revealed a high surface area of 243.4 m^2/g, a total pore volume of 0.9309 cm^3/g, and an average pore size of 9.37 nm, as determined by Brunauer-Emmett-Teller (BET) analysis, indicating a highly porous structure favorable for pesticide adsorption.

3.2.4 *FTIR spectroscopy*

The FTIR spectra of CMC, MGO-NPs, and CMC-MGO-NPs are presented in Figure 5a-c. The FTIR spectrum of CMC (Figure 5a) exhibited a broad peak at 3,362 cm^{-1}, corresponding to O-H stretching vibrations, while the band at 2,925 cm^{-1} was attributed to C-H stretching. Strong peaks at 1,617 cm^{-1} and 1,426 cm^{-1} confirmed the presence of asymmetric and symmetric -COO^- stretching from carboxylate groups in CMC, and the peak at 1,062 cm^{-1} was assigned to C-O stretching in the pyranose ring and primary alcohols of the cellulose backbone.[43]

Figure 5b displays the FTIR spectrum of MGO-NPs, revealing key functional groups and structural features. A strong peak at 3,410 cm^{-1} corresponds to O-H stretching vibrations.[12] However, peaks at 1,629 cm^{-1} (C=O), 1,179 cm^{-1} (C=C), and 1,098 cm^{-1} (C-H) further confirm organic moieties.[44] Additionally, two distinct bands at 644 and 677 cm^{-1} signify the spinel structure of MGO-NPs, attributed to Fe-O bonds in their framework.[12]

The FTIR spectrum of CMC-MGO-NPs (Figure 5c) displayed a broad band at 3,442 cm^{-1}, corresponding to O-H stretching and hydrogen bonding. A peak at 2,927 cm^{-1} indicated C-H stretching from β (1 → 4)-linked D-glucose units in cellulose. The asymmetric and symmetric vibrations of carboxylate groups appeared at 1,633 cm^{-1} and 1,462 cm^{-1}, respectively, while peaks between 1,024-1,119 cm^{-1} were assigned to C-O- stretching in the polysaccharide backbone.[12] The spectrum revealed a peak at 620 cm^{-1}, corresponding to Fe-O bond stretching. Upon CMC modification, key peaks emerged at 3,442 cm^{-1} (O-H stretching), 1,633 cm^{-1} (COO^- group), and 1,427 cm^{-1} (-CH_2 scissoring vibration). The characteristic asymmetric vibration of COO^- in CMC is observed at approximately 1,617 cm^{-1} (Figure 5a). In the crosslinked CMC-MGO-NPs composite, this peak shift to 1,633 cm^{-1} (Figure 5c). This small but measurable shift to higher wavenumber is a classic indicator of ionic crosslinking. It suggests a change in the ionic environment of the carboxylate groups due to their complexation with Ca^{2+} ions (chelation), which affects the C=O bond strength, rather than the formation of a new covalent C-O-Ca bond which would present a more dramatic shift and a new peak. These findings confirm the successful interaction between GO and CMC via hydrogen bonding, indicating effective integration of the two components.[45]

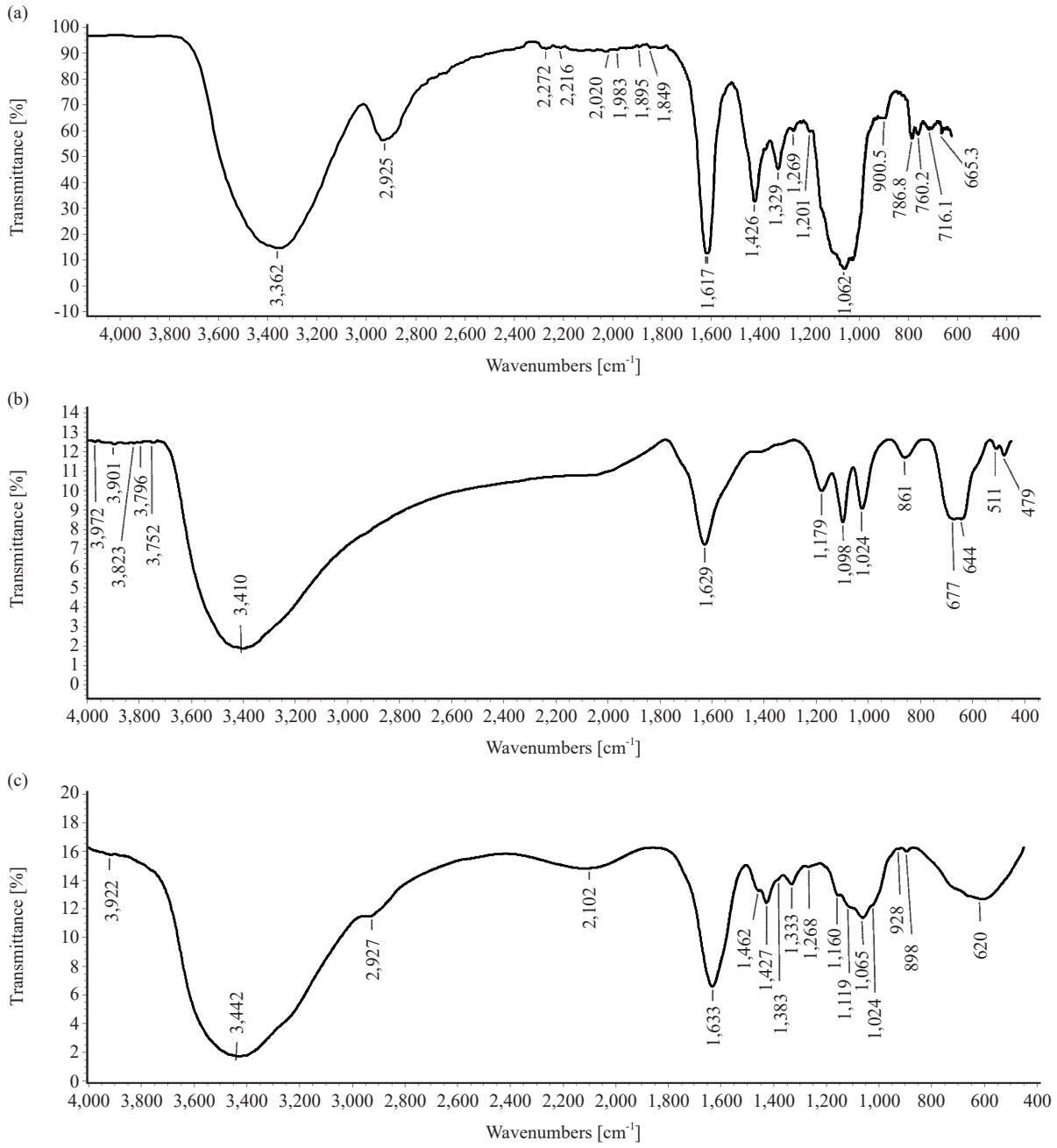

Figure 5. FTIR spectra of CMC (a), MGO-NPs (b), and CMC-MGO-NPs-2 (c)

3.3 *Removal of pesticides by CMC-MNPs-2*

The removal of tested pesticides by CMC-MGO-NPs-2 under varying parameters is shown in Tables 3-5. As indicated in Table 3, the removal efficiency of florasulam using CMC-MGO-NPs-2 varied significantly across experimental runs (82.18-93.82%). The highest removal rates were observed in runs 2, 3, 5, and 7 (90.18-93.82%), followed by moderate efficiency in runs 6, 11, and 13 (86.18-89.31%). The lowest removal (82.18-85.45%) occurred in runs 1, 4, 8, 9, 10, and 12. In terms of adsorption capacity, runs 1, 4, and 10 showed the highest values (9.95-10.09 mg/g), while runs 2, 5, 6, 8, 9, 12, and 13 exhibited moderate capacity (3.01-3.66 mg/g). The lowest adsorption (1.05-1.15 mg/g) was recorded in runs 3, 7, and 11. The Enrichment Factor (EF) for florasulam was highest in runs 1, 4, 8, 9, 10, and 12 (0.15-0.18), moderate in runs 6, 11, and 13 (0.11-0.14), and lowest in runs 2, 3, 5, and 7 (0.06-0.10).

Table 3. Adsorption performance of CMC-MGO-NPs-2 for florasulam

Run	Added amount (μg) ± SE	Found amount (μg) ± SE	Adsorbed amount (μg) ± SE	Non-extracted amount (μg) ± SE	Removal (%) ± SE	Adsorption capacity (mg/g) ± SE	Enrichment factor ± SE
1	150	23.83 ± 1.35	123.00 ± 0.77	3.17 ± 0.58	83.91^{d} ± 0.91	9.95^{a} ± 0.11	0.16^{a} ± 0.009
2	150	11.00 ± 1.06	136.33 ± 0.39	2.67 ± 0.67	92.58^{ab} ± 0.72	3.66^{b} ± 0.03	0.07^{cd} ± 0.007
3	50	2.83 ± 0.39	46.67 ± 0.58	0.50 ± 0.19	93.82^{a} ± 0.84	1.15^{e} ± 0.01	0.06^{d} ± 0.008
4	150	22.00 ± 0.48	126.00 ± 0.96	2.00 ± 1.45	85.15^{cd} ± 0.33	10.09^{a} ± 0.04	0.15^{ab} ± 0.003
5	150	12.50 ± 0.96	134.67 ± 0.96	2.83 ± 1.93	91.56^{ab} ± 0.65	3.62^{b} ± 0.03	0.08^{cd} ± 0.007
6	150	15.83 ± 1.54	132.00 ± 0.58	2.17 ± 0.96	89.31^{bc} ± 1.04	3.53^{bc} ± 0.04	0.11^{bc} ± 0.010
7	50	4.50 ± 0.58	43.67 ± 0.39	1.83 ± 0.19	90.18^{ab} ± 1.26	1.10^{e} ± 0.02	0.10^{cd} ± 0.013
8	50	6.83 ± 0.77	42.33 ± 0.39	0.83 ± 0.39	85.09^{cd} ± 1.68	3.12^{d} ± 0.06	0.15^{ab} ± 0.017
9	50	6.67 ± 0.67	41.33 ± 0.58	2.00 ± 0.10	85.45^{cd} ± 1.47	3.13^{d} ± 0.05	0.15^{ab} ± 0.015
10	150	23.50 ± 0.77	125.67 ± 1.16	0.83 ± 0.39	84.14^{d} ± 0.52	9.97^{a} ± 0.06	0.16^{a} ± 0.005
11	50	6.33 ± 0.29	42.67 ± 0.19	1.00 ± 0.10	86.18^{cd} ± 0.63	1.05^{e} ± 0.01	0.14^{ab} ± 0.006
12	50	8.17 ± 0.39	40.33 ± 0.77	1.50 ± 0.39	82.18^{d} ± 0.84	3.01^{d} ± 0.03	0.18^{a} ± 0.008
13	100	10.83 ± 0.96	87.00 ± 1.16	2.17 ± 0.19	88.77^{bc} ± 1.00	3.43^{c} ± 0.04	0.11^{bc} ± 0.010

Values represent the mean ± Standard Error (SE) of three independent replicates. Different uppercase letters within a column indicate statistically significant differences between runs ($P \leq 0.05$, ANOVA with Student-Newman-Keuls test)

Table 4. Adsorption performance of CMC-MGO-NPs-2 for metalaxyl

Run	Added amount (μg) ± SE	Found amount (μg) ± SE	Adsorbed amount (μg) ± SE	Non-extracted amount (μg) ± SE	Removal (%) ± SE	Adsorption capacity (mg/g) ± SE	Enrichment factor ± SE
1	150	104.43 ± 2.85	43.35 ± 1.14	2.22 ± 1.71	30.72^{h} ± 1.89	3.70^{c} ± 0.23	0.69^{b} ± 0.019
2	150	24.63 ± 1.14	123.15 ± 1.71	2.22 ± 0.57	83.66^{b} ± 0.76	3.36^{d} ± 0.03	0.16^{h} ± 0.008
3	50	4.93 ± 0.57	43.35 ± 1.14	1.72 ± 0.57	88.10^{a} ± 1.38	0.97^{h} ± 0.02	0.12^{i} ± 0.014
4	150	86.70 ± 1.14	59.11 ± 1.14	4.19 ± 2.28	42.48^{f} ± 0.76	5.12^{a} ± 0.09	0.58^{d} ± 0.008
5	150	27.59 ± 0.57	119.21 ± 0.57	3.20 ± 1.14	81.70^{b} ± 0.38	3.28^{d} ± 0.02	0.18^{h} ± 0.004
6	150	38.92 ± 0.85	108.37 ± 1.14	2.71 ± 0.28	74.18^{c} ± 0.57	2.98^{e} ± 0.02	0.26^{g} ± 0.006
7	50	9.36 ± 0.85	39.41 ± 1.14	1.23 ± 0.28	77.38^{c} ± 2.06	0.85^{h} ± 0.02	0.23^{g} ± 0.021
8	50	16.75 ± 1.14	32.51 ± 0.57	0.74 ± 0.57	59.52^{e} ± 2.75	1.97^{g} ± 0.09	0.40^{e} ± 0.028
9	50	13.79 ± 0.57	35.47 ± 1.14	0.74 ± 0.57	66.67^{d} ± 1.38	2.21^{g} ± 0.05	0.33^{f} ± 0.014
10	150	93.10 ± 1.42	54.19 ± 1.71	2.71 ± 0.28	38.24^{g} ± 0.94	4.61^{b} ± 0.11	0.62^{c} ± 0.009
11	50	11.33 ± 0.28	36.45 ± 0.57	2.22 ± 0.28	72.62^{c} ± 0.69	0.80^{h} ± 0.01	0.27^{g} ± 0.007
12	50	31.03 ± 0.85	16.75 ± 1.71	2.22 ± 0.85	25.00^{i} ± 2.06	0.83^{h} ± 0.07	0.75^{a} ± 0.021
13	100	36.95 ± 0.85	62.07 ± 0.57	0.99 ± 0.28	63.59^{de} ± 0.84	2.58^{f} ± 0.03	0.36^{ef} ± 0.008

Values represent the mean ± Standard Error (SE) of three independent replicates. Different uppercase letters within a column indicate statistically significant differences between runs ($P \leq 0.05$, ANOVA with Student-Newman-Keuls test)

Table 5. Adsorption performance of CMC-MGO-NPs-2 for thiamethoxam

Run	Added amount (µg) ± SE	Found amount (µg) ± SE	Adsorbed amount (µg) ± SE	Non-extracted amount (µg) ± SE	Removal (%) ± SE	Adsorption capacity (mg/g) ± SE	Enrichment factor ± SE
1	150	141.06 ± 0.19	7.50 ± 0.77	1.44 ± 0.96	2.30^{kl} ± 0.13	0.27^{fg} ± 0.02	0.98^{a} ± 0.001
2	150	110.88 ± 0.96	38.67 ± 1.15	0.45 ± 0.19	23.20^{b} ± 0.66	0.89^{a} ± 0.03	0.77^{k} ± 0.007
3	50	33.76 ± 0.29	14.79 ± 0.38	1.44 ± 0.10	28.46^{a} ± 0.61	0.36^{e} ± 0.01	0.72^{l} ± 0.006
4	150	137.74 ± 0.38	11.48 ± 0.77	0.78 ± 0.38	4.59^{ij} ± 0.27	0.53^{c} ± 0.03	0.95^{cd} ± 0.003
5	150	114.20 ± 0.58	35.36 ± 0.77	0.45 ± 0.19	20.91^{c} ± 0.40	0.80^{b} ± 0.02	0.79^{j} ± 0.004
6	150	123.32 ± 1.05	24.74 ± 0.77	1.94 ± 0.29	14.59^{e} ± 0.73	0.56^{c} ± 0.03	0.85^{h} ± 0.007
7	50	38.57 ± 0.38	10.48 ± 0.58	0.95 ± 0.19	18.27^{d} ± 0.81	0.23^{g} ± 0.01	0.82^{i} ± 0.008
8	50	44.38 ± 0.29	4.84 ± 0.77	0.78 ± 0.48	5.97^{i} ± 0.61	0.23^{g} ± 0.02	0.94^{d} ± 0.006
9	50	43.05 ± 0.10	6.50 ± 0.19	0.45 ± 0.29	8.78^{h} ± 0.20	0.33^{ef} ± 0.01	0.91^{e} ± 0.002
10	150	138.91 ± 0.48	10.48 ± 0.58	0.61 ± 0.10	3.79^{jk} ± 0.33	0.44^{d} ± 0.04	0.96^{bc} ± 0.003
11	50	42.22 ± 0.19	7.16 ± 0.58	0.61 ± 0.38	10.54^{g} ± 0.41	0.13^{h} ± 0.01	0.89^{f} ± 0.004
12	50	46.37 ± 0.10	2.85 ± 0.38	0.78 ± 0.48	1.76^{l} ± 0.20	0.07^{h} ± 0.01	0.98^{ab} ± 0.002
13	100	88.33 ± 0.96	11.14 ± 1.34	0.53 ± 0.38	12.20^{f} ± 0.95	0.49^{cd} ± 0.04	0.88^{g} ± 0.010

Values represent the mean ± Standard Error (SE) of three independent replicates. Different uppercase letters within a column indicate statistically significant differences between runs ($P \leq 0.05$, ANOVA with Student-Newman-Keuls test)

A Pareto chart (Figure 6a) was used to analyze the key factors affecting florasulam adsorption by CMC-MGO-NPs-2. The adsorbent amount had the most significant impact ($\alpha = 0.05$), while pH, agitation time, ionic strength, temperature, and pesticide concentration were non-significant (values below the reference line of 2.447). The removal prediction model is given in equation (10).

$$\text{Removal (\%)} = 76.05 + 0.0125\ \text{Pesticide concentration} + 0.1257\ \text{Adsorbent amount}$$

$$+ 0.0299\ \text{Temperature} + 0.436\ \text{pH} + 0.0766\ \text{Agitation time} - 0.145\ \text{Ionic strength}$$

$$S = 1.80 \text{ and } R^2 = 88.18\% \quad (10)$$

It can be seen that the ionic strength factor had a negative coefficient indicating a decrease in adsorption with the increase of this factor. However, other factors presented a positive coefficient.

The data in Table 4 showed that the removal efficiency of metalaxyl by CMC-MGO-NPs-2 varied widely (25.00-88.10%), averaging 61.84%, with the highest efficiencies in runs 2, 3, 5, 6, 7, and 11 (72.62-88.10%) and the lowest in runs 1, 4, 10, and 12 (25.00-42.48%). Adsorption capacity was highest in runs 1, 4, and 10 (3.70-5.12 mg/g), moderate in runs 2, 5, 6, and 13 (2.58-3.36 mg/g), and lowest in runs 3, 7, 8, 9, 11, and 12 (0.80-1.97 mg/g). Conversely, EF values were highest in runs 1, 4, 10, and 12 (0.58-0.75), moderate in runs 8, 9, and 13 (0.33-0.40), and lowest in runs 2, 3, 5, 6, 7, and 11 (0.12-0.27).

A Pareto chart (Figure 6b) revealed that adsorbent amount, pH, and agitation time were the most significant factors affecting metalaxyl removal by CMC-MGO-NPs-2 ($\alpha = 0.05$), while pesticide concentration, temperature, and ionic strength had negligible influence. This analysis indicates that metalaxyl removal efficiency can be predicted using the

proposed model (equation (11)).

$$\text{Removal (\%)} = -5.3 - 0.1277\ \text{Pesticide concentration} + 0.7167\ \text{Adsorbent amount} + 0.025\ \text{Temperature} + 3.44\ \text{pH} + 0.638\ \text{Agitation time} + 0.048\ \text{Ionic strength}$$

$$S = 7.37 \text{ and } R^2 = 93.92\% \quad (11)$$

The pesticide concentration factor negatively impacted adsorption, meaning it decreased as the concentration factor increased. However, other factors had a positive influence.

The use of CMC-MGO-NPs-2 for removing thiamethoxam through adsorption resulted in a wide range of efficiencies, between a minimum of 1.76% to a maximum of 28.46% (Table 5). While some runs achieved high removal efficiencies (23.20%-28.46%) for thiamethoxam with these nanoparticles, the overall average (11.95%) suggests limited effectiveness. Runs 2, 3, 5, and 7 performed best, while runs 6, 11, and 13 showed moderate removal. The remaining runs (1, 4, 8, 9, 10, and 12) had very low removal efficiencies (1.76-8.78%). An analysis of thiamethoxam adsorption onto CMC-MGO-NPs-2 revealed high adsorption capacity (0.89 and 0.80 mg/g) in runs 2 and 5. Runs 3, 4, 6, 9, 10, and 13 demonstrated moderate adsorption capacity (0.33-0.56 mg/g), whereas runs 1, 7, 8, 11, and 12 had the lowest (0.07-0.27 mg/g). For thiamethoxam removal, runs 1, 4, 8, 9, 10, and 12 achieved the highest EF (0.91-0.98), runs 6, 11, and 13 showed moderate EF (0.85-0.89), and runs 2, 3, 5, and 7 had the lowest EF (0.72-0.79).

A Pareto chart (Figure 6c) revealed that the adsorbent amount was the most influential factor in thiamethoxam removal by CMC-MGO-NPs-2, with statistical significance (α = 0.05). Ionic strength, agitation time, pH, temperature, and pesticide concentration all had minimal influence due to values falling below the reference line (2.447, α = 0.05). This analysis suggests a model (equation (12)) might be used to predict thiamethoxam removal efficiency based on these factors.

$$\text{Removal (\%)} = -10.56 - 0.0147\ \text{Pesticide concentration} + 0.2959\ \text{Adsorbent amount} + 0.0289\ \text{Temperature} + 0.846\ \text{pH} + 0.182\ \text{Agitation time} - 0.367\ \text{Ionic strength}$$

$$S = 4.41 \text{ and } R^2 = 86.90\% \quad (12)$$

From this model, it can be seen that the adsorption efficiency was negatively affected by both pesticide concentration and ionic strength, with a decrease observed as their levels increased. However, other factors contributed positively to the adsorption process.

The reusability of CMC-MGO-NPs-2 was evaluated in preliminary experiments. Following a regeneration process involving methanol washing and drying, the nanoparticles were reused for pesticide adsorption. These initial studies, the data for which are not presented here, revealed that the adsorbent maintains its adsorption capacity through multiple cycles, suggesting strong potential for repeated use. A comprehensive analysis of the adsorbent's regenerative capacity and long-term stability will be the focus of future work, which will include optimization of elution solvents and a detailed evaluation over consecutive adsorption-desorption cycles.

The development of efficient and sustainable adsorbents for pesticide remediation is a critical challenge in environmental science. This study successfully synthesized CMC-MGO-NPs, and CMC-MGO-NPs-2 demonstrated its exceptional efficacy in removing different pesticides from aqueous solutions. The high removal efficiencies (82.18-93.82%) achieved for florasulam, and (25.00-88.10%) for metalaxyl, underscore the effectiveness of the CMC-MGO-NPs-2 design. This performance is markedly superior to many reported adsorbents, such as activated carbons[46] and unmodified graphene oxide,[47] which often suffer from lower adsorption capacities or poor selectivity. The exceptional performance is attributed to a synergistic effect between the components of the nanocomposite.

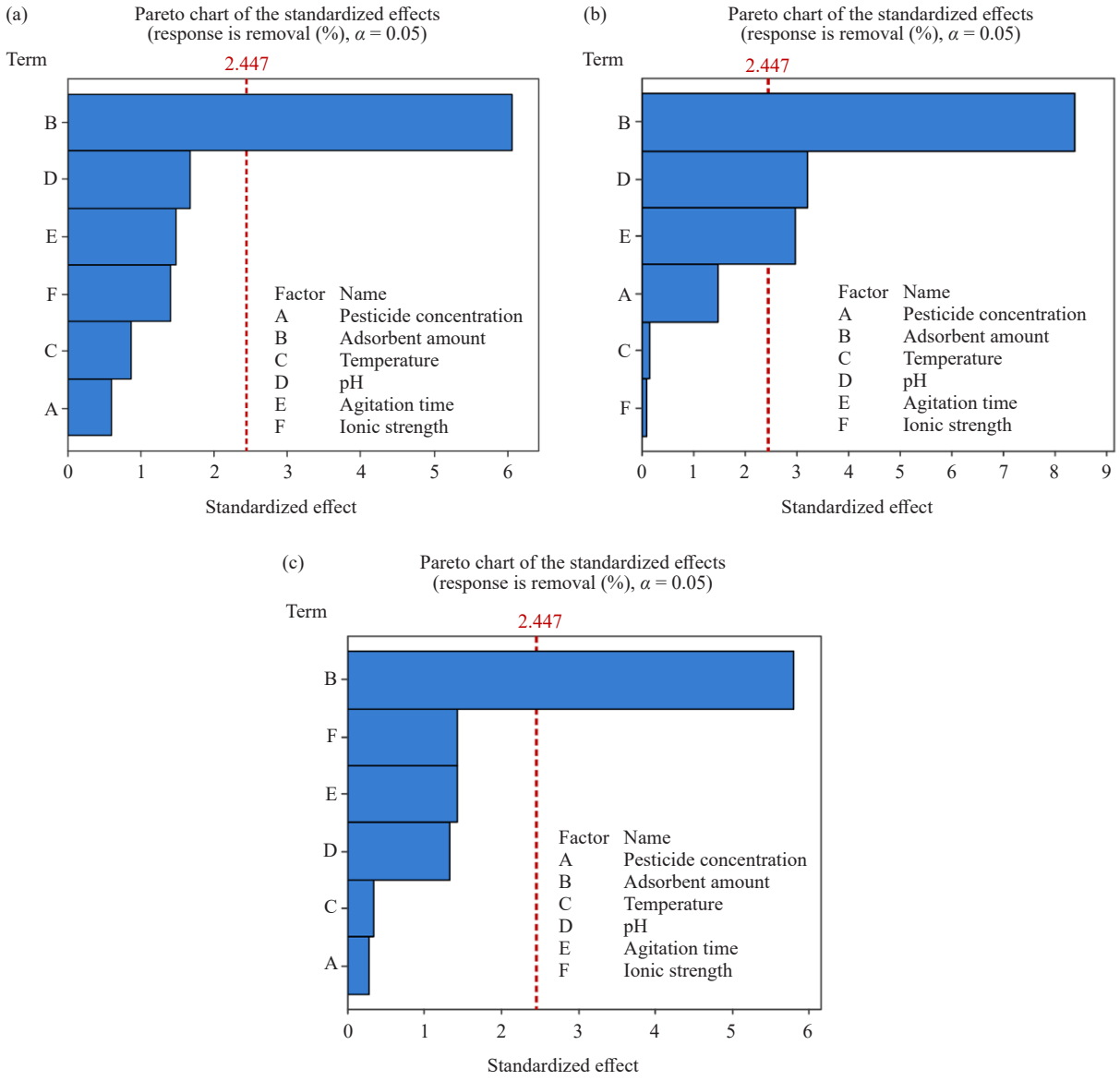

Figure 6. Pareto charts of the standardized effects of pesticide concentration, adsorbent amount, temperature, pH, agitation time, and ionic strength on the adsorption of florasulam (a), metalaxyl (b), and thiamethoxam (c) on CMC-MGO-NPs-2 (response is removal (%), $\alpha = 0.05$)

Overall, CMC-MGO-NPs offer a promising approach to pesticide removal due to their high adsorption capacity, magnetic separation, and potential biocompatibility.[12] The present results demonstrated low removal efficiencies (1.76-28.46%) for thiamethoxam by CMC-MGO-NPs-2. This poor adsorption is attributed to the high hydrophilicity and polarity of thiamethoxam, as indicated by its low octanol-water partition coefficient ($\log P$ = -1.16). These properties diminish its affinity for the predominantly hydrophobic adsorbent surface, limiting key adsorption mechanisms such as electrostatic attraction and hydrogen bonding. In contrast, the higher removal efficiencies observed for florasulam and metalaxyl ($\log P$ = 1.29 and 2.15, respectively) are consistent with their greater hydrophobicity, which favors partitioning onto the nonpolar adsorbent surface via hydrophobic interactions. Previous investigations have documented the efficacy of CMC-MGO-NPs as adsorbents for pesticide remediation in aqueous environments. These nanocomposites have demonstrated a high adsorption capacity, facilitating the effective removal of specific pesticides, including atrazine and chlorpyrifos, from aqueous solutions.[12,48]

3.4 *Adsorption kinetic and isotherm studies*

3.4.1 *Kinetic studies*

Kinetic analysis revealed the time-dependent adsorption behavior of florasulam, metalaxyl, and thiamethoxam onto CMC-MGO-NPs-2. The process is characterized by an initial rapid uptake phase, attributable to the high availability of unoccupied active sites on the adsorbent surface. As depicted in Figure 7, this initial rate subsequently decays, a phenomenon consistent with the gradual saturation of these binding sites. Equilibrium attainment was pesticide-specific, occurring at 15, 20, and 25 min for florasulam, metalaxyl, and thiamethoxam, respectively (Figure 7a-c). These divergent saturation times indicate that while the initial adsorption mechanism is similarly rapid for all three compounds, their subsequent interaction kinetics, likely influenced by molecular size, diffusion rates, and binding affinity, govern the time required to reach equilibrium.

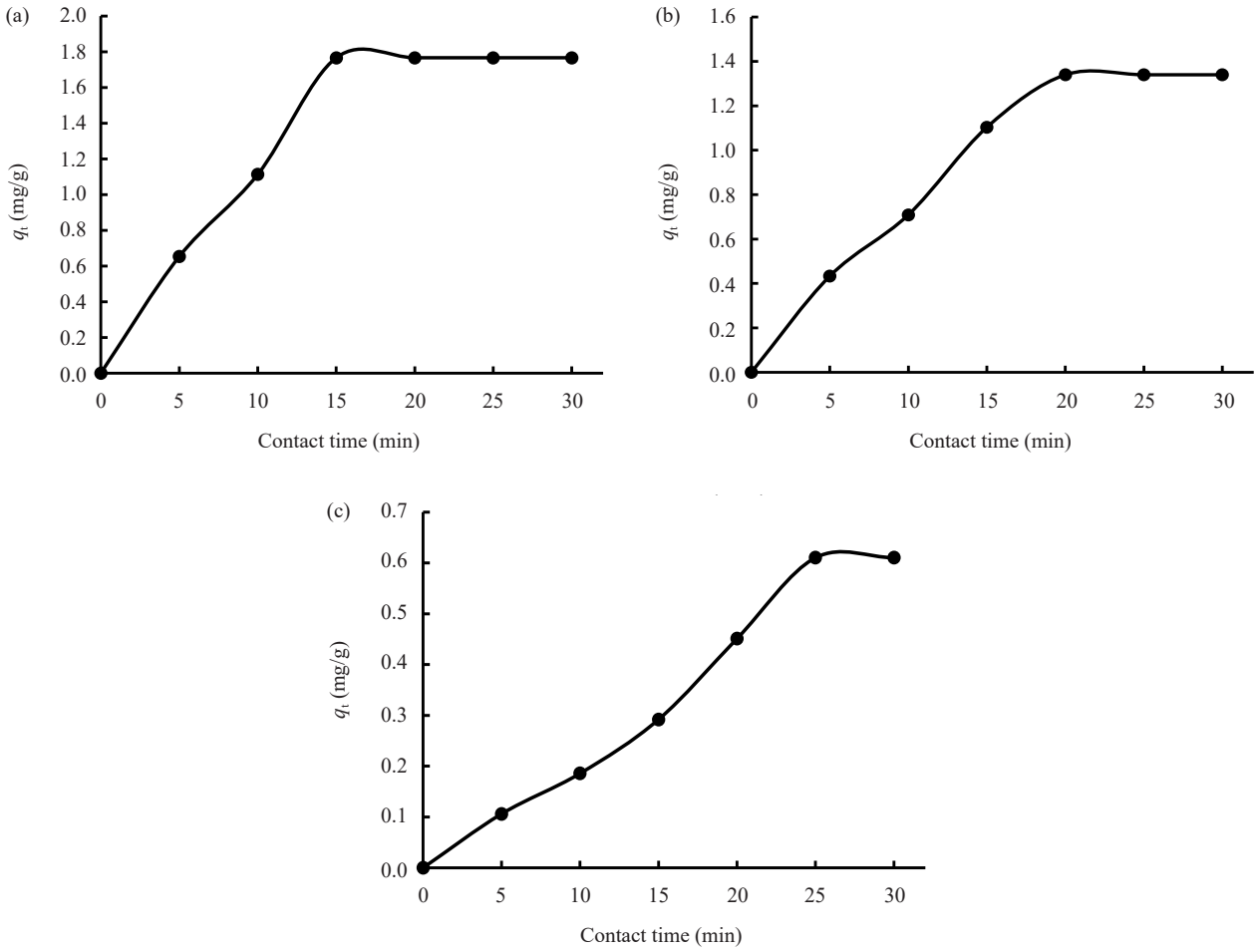

Figure 7. Effect of initial pesticides concentrations (50 µg/mL) and contact time on the adsorption of ((a): Florasulam, (b): Metalaxyl, (c): Thiamethoxam) by CMC-MGO-NPs (Condition: 50 mg of of adsorbent in 2 mL of water at 150 rpm for 30 min)

In this study, a linear plot was used to determine the rate constant (K_1) and the amount of adsorbate molecules at equilibrium (q_e), which represent the adsorption capacity for pseudo-first-order and pseudo-second-order kinetic models, respectively (Figure 8a-c). The pseudo-first-order model provided the strongest fit for florasulam and metalaxyl, as indicated by near-perfect and high R^2 values of 1.00 and 0.93, respectively. In contrast, the pseudo-second-order model was a poor descriptor for all analytes, particularly for thiamethoxam (R^2 = 0.16). The adsorption kinetics for thiamethoxam were best explained by the intraparticle diffusion model (R^2 = 0.95), suggesting a diffusion-controlled

process. Consequently, the primary adsorption mechanism is chemisorption for florasulam and metalaxyl, while pore diffusion dominates for thiamethoxam.

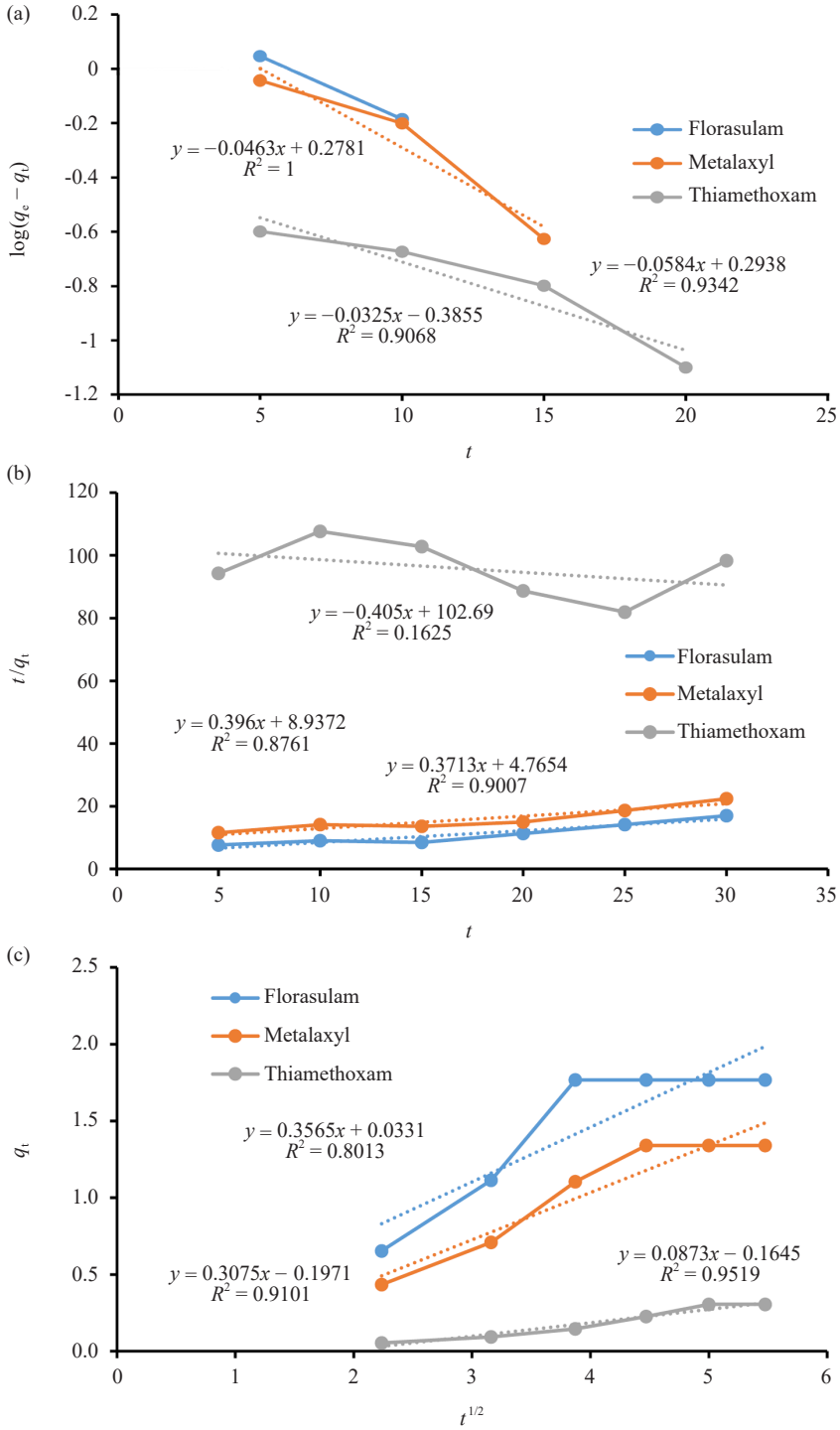

Figure 8. Kinetic models ((a): Pseudo-first-order, (b): Pseudo-second-order, (c): Intraparticle diffusion) on the adsorption of florasulam, metalaxyl, and thiamethoxam by CMC-MGO-NPs-2 (Condition: 50 mg of adsorbent in 2 mL water containing of 50 µg/mL from each pesticide at 150 rpm at different times 5, 10, 15, 20, 25, and 30 min)

The adsorption kinetics of florasulam, metalaxyl, and thiamethoxam onto CMC-MGO-NPs-2 were rigorously evaluated (Table 6). Analysis of the Sum of Squared Errors (% SSE) decisively identified the pseudo-second-order model as the primary mechanism, yielding near-perfect fits (% SSE: 0.17-0.27%). While the intraparticle diffusion model also demonstrated strong correlation (% SSE: 0.15-0.27%), confirming its role in the process, the pseudo-first-order model proved to be a poor descriptor of the kinetics (% SSE: 5.22-21.52%).

Table 6. Kinetic model parameters for adsorption of florasulam, metalaxyl, and thiamethoxam pesticides on CMC-MGO-NPs-2

Pesticide	Pseudo-first order				Pseudo-second order				Intraparticle diffusion			
	K_1	q_e	R^2	% SSE	K_2	q_e	R^2	% SSE	K_{id}	C_{id}	R^2	% SSE
Florasulam	0.11	1.90	1.00	9.54	0.03	2.69	0.90	0.27	0.36	0.03	0.80	0.27
Metalaxyl	0.13	1.97	0.93	21.52	0.02	2.53	0.88	0.25	0.31	-0.20	0.91	0.25
Thiamethoxam	0.08	2.43	0.91	5.22	0.002	-2.47	0.16	0.17	0.09	-0.16	0.95	0.17

K_1: is the rate constant of pseudo-first order kinetic. q_e: is the amount of pesticides adsorbed at equilibrium. K_2: is the rate constant of pseudo-second-order kinetic. K_{id}: is the rate constant of intraparticle diffusion kinetic. C_{id}: is the intercept related to the thickness of the boundary layer. R^2: is the correlation coefficient. % SSE: is the percentage of the Sum of Squared Errors

The binding kinetics of florasulam, metalaxyl, and thiamethoxam to CMC-MGO-NPs-2 were also studied using the intraparticle diffusion model ($q_t = C_{id} + K_{id} t^{1/2}$). In this model, the slope (K_{id}) indicates the diffusion rate within the particles, while the intercept (C_{id}) reflects boundary layer thickness. Results showed a two-stage process: pesticides were first quickly adsorbed onto the nanoparticle surface, followed by slower diffusion into the particle interior.[49]

3.4.2 *Isotherm studies*

Three adsorption isotherm models (Freundlich, Langmuir, and Temkin) were tested to describe how pesticides bind to CMC-MGO-NPs-2, with results shown in Figures 9a-c and Table 7. The goodness of fit was measured using R^2 values (closer to 1.0 indicates better fit). The Langmuir model best described the adsorption of florasulam and thiamethoxam (R^2 = 0.95 for both), while the Freundlich model was most suitable for metalaxyl (R^2 = 0.99). The Temkin model generally showed poorer fits, particularly for florasulam and thiamethoxam. The Freundlich isotherm model best described the adsorption of florasulam, metalaxyl, and thiamethoxam onto CMC-MGO-NPs-2, as evidenced by significantly lower % SSE values (0.16%, 0.02%, and 0.06%, respectively) compared to the Langmuir (0.21%, 0.05%, and 0.09%) and Temkin (0.20%, 0.04%, and 0.09%) models. This indicates that the Freundlich model more accurately represents the adsorption mechanisms of these pesticides, likely due to its suitability for heterogeneous surfaces and multilayer adsorption behavior.

Table 7. Isotherm model parameters for adsorption of florasulam, metalaxyl, and thiamethoxam pesticides on CMC-MGO-NPs-2

Pesticide	Freundlich				Langmuir				Temkin			
	K_f	$1/n$	R^2	% SSE	b_1	q_m	R^2	% SSE	b_2	K_T	R^2	% SSE
Florasulam	0.53	0.51	0.90	0.16	0.08	4.20	0.95	0.21	2.39	0.66	0.82	0.20
Metalaxyl	0.34	0.45	0.99	0.02	0.04	3.18	0.96	0.05	2.96	0.24	0.96	0.04
Thiamethoxam	0.004	1.21	0.94	0.06	0.000	-18.48	0.95	0.09	3.53	0.05	0.76	0.09

K_f: is the Freundlich isotherm constant. K_T: is the maximum binding energy. $1/n$: is the adsorption intensity. R^2: is the correlation coefficient. % SSE: is the percentage of the Sum of Squared Errors. b_1: is the Langmuir isotherm constant. b_2: is the Temkin isotherm constant. q_m: is the maximum adsorption capacity on a monolayer

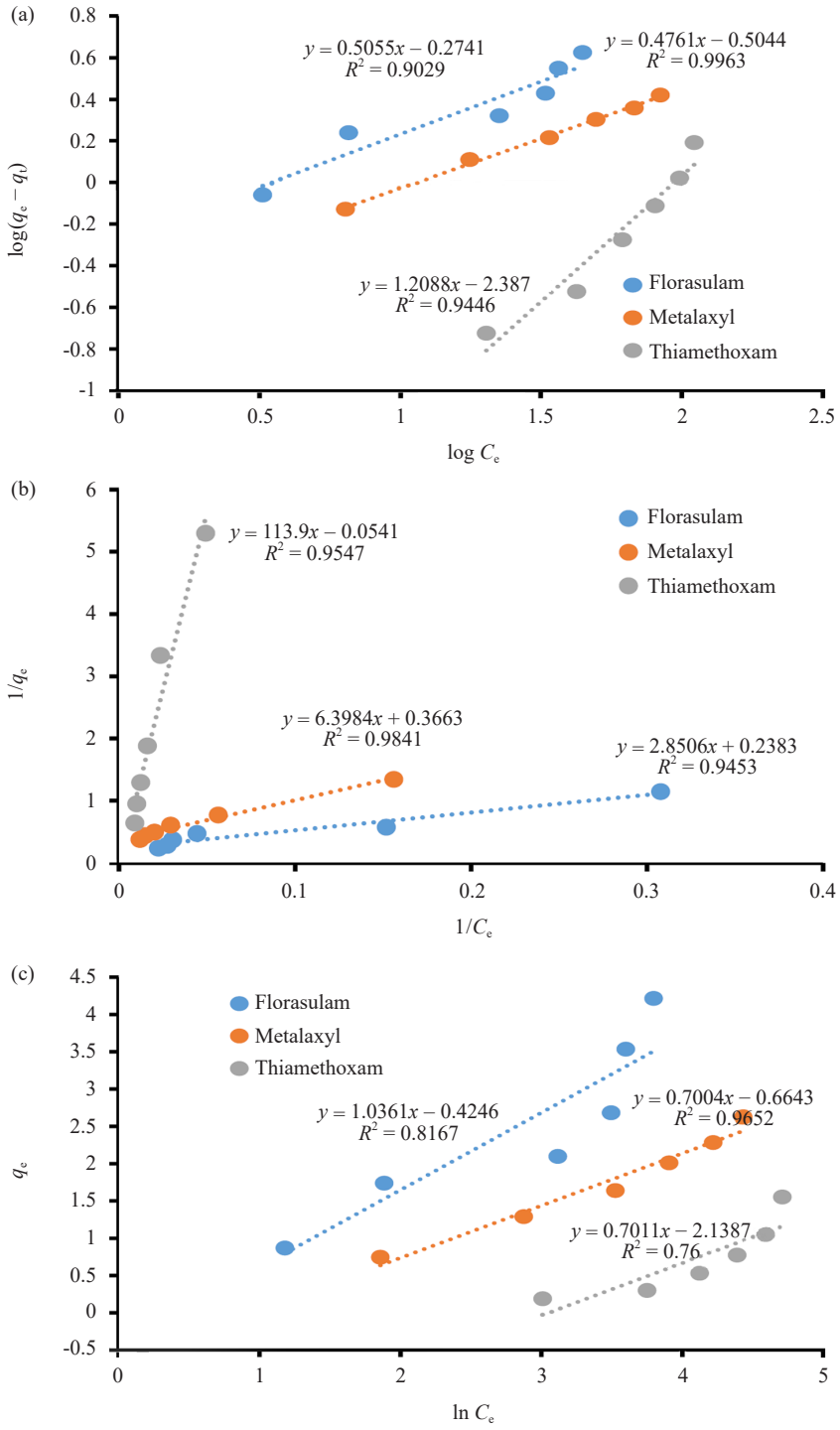

Figure 9. Isotherm models ((a): Freundlich, (b): Langmuir, (c): Temkin) on the adsorption of florasulam, metalaxyl, and thiamethoxam by CMC-MGO-NPs-2 (Condition: 50 mg of adsorbent in 2 mL water containing of 25, 50, 75, 100, 125, and 150 µg/mL from each pesticide at 150 rpm at equilibrium time)

Isotherm models (Freundlich, Langmuir, and Temkin) describe how molecules (adsorbates) distribute themselves on solid surfaces (adsorbents) at equilibrium and constant temperature. Each model makes different assumptions about surface uniformity and binding strength. The Freundlich isotherm, the most flexible of the three, treats the surface as energetically heterogeneous and allows multilayer adsorption, with the highest-energy sites occupied first.[50] In contrast,

the Langmuir isotherm is based on the assumption that the surface is uniform, with every site having the same energy. It proposes that only a single layer of adsorbate can form on the surface.[51] Finally, the Temkin isotherm takes into account the attractive interactions between the adsorbate and the adsorbent, making it particularly useful for situations where a chemical bond, or chemisorption, occurs on a non-uniform surface.[52]

4. Conclusion

In recent years, nanoparticle-based adsorption has gained significant attention for water treatment. This study demonstrates the successful synthesis of cost-effective CMC-MGO-NPs. Spectroscopic analysis confirms that these nanoparticles exhibit pesticide removal efficiency, attributable to their anionic functional groups, porous structure, and surface roughness. By systematically adjusting parameters like pesticide concentration, adsorbent amount, temperature, pH, agitation time, and ionic strength, the adsorption process was optimized, demonstrating the strong suitability of CMC-MGO-NPs-2. In addition, the adsorption mechanism of pesticides onto CMC-MGO-NPs-2 was investigated through kinetic and isotherm modelling. The CMC-MGO-NPs-2 exhibited high adsorption efficiency for florasulam (93.82%) and metalaxyl (88.10%), demonstrating a strong affinity for these pesticides. In contrast, a significantly lower efficiency for thiamethoxam (28.46%) revealed distinct selectivity in the adsorption process. CMC-MGO-NPs have great potential to be used as environmentally friendly, highly effective, and stable absorbents. Therefore, these nanoparticles offer promising and excellent adsorbent materials for the sustainable application in wastewater purification process. While nanotechnology offers promising methods for the wastewater purification process, including removing pesticides and other pollutants, large-scale application requires further study. Further research is essential to assess the potential risks of nanomaterials to both the environment and human health.

Availability of data and materials

All data generated or analyzed during this study are included in this article. Also, the related datasets are available from the corresponding author upon reasonable request.

Funding

Financial support for this research was provided by the Science and Technology Development Fund (STDF, Project 37143) and the Misr El Kheir Foundation (STI Program, Project LGA05130114).

Acknowledgments

The authors gratefully acknowledge Prof. Dr. Ahmed F. El-Aswad (Department of Pesticide Chemistry and Technology, Faculty of Agriculture, Alexandria University, Egypt) for his invaluable advice and assistance with the kinetic and isothermal experiments.

Conflict of interest

The authors have no conflicts of interest to disclose.

References

[1] Ratnadass, A.; Deberdt, P.; Martin, T.; Sester, M.; Deguine, J. P. Impacts of crop protection practices on human

infectious diseases: agroecology as the preferred strategy to integrate crop plant health within the extended "one health" framework. In *One Health: Human, Animal, and Environment Triad*; Vithanage, M., Prasad, M. N. V., Eds.; Wiley: Hoboken, NJ, 2023; pp 287-308.
[2] Hamed, A. S. A.; Hidayah, N. Global trade and pesticide use. In *The Interplay of Pesticides and Climate Change: Environmental Dynamics and Challenges*; Babaniyi, B. R., Babaniyi, E. E., Eds.; Springer: New York, NY, 2025; pp 111-126.
[3] Sweeney, K. Present and future approaches to urban pest management: a global pesticide regulatory perspective. In *Urban Pest Management: An Environmental Perspective*; CABI: London, UK, 2023; pp 121-141.
[4] Gul, S.; Chashoo, H. F.; Hanief, F.; Abubakr, A.; Malik, M. M.; Hamid, I. Pesticide biomagnification: A comprehensive exploration of environmental dynamics and human health implications. In *Food Security, Nutrition and Sustainability Through Aquaculture Technologies*; Springer: Cham, 2025; pp 299-309.
[5] Tang, F. H. M.; Lenzen, M.; McBratney, A.; Maggi, F. Risk of pesticide pollution at the global scale. *Nat. Geosci*. **2021,** *14*, 206-210.
[6] Mansour, S. A. Environmental impact of pesticides in Egypt. *Rev. Environ. Contam. Toxicol*. **2008,** *196*, 1-51.
[7] Eissa, F.; Al-Sisi, M.; Ghanem, K. Occurrence, human health, and ecotoxicological risk assessment of pesticides in surface waters of the River Nile's Rosetta Branch, Egypt. *Environ. Sci. Pollut. Res*. **2021,** *28*, 55511-55525.
[8] European Food Safety Authority. Conclusion on the peer review of the pesticide risk assessment of the active substance florasulam. *EFSA J*. **2015,** *13*, 3984.
[9] European Food Safety Authority; Álvarez, F.; Arena, M.; Auteri, D.; Leite, S. B.; Binaglia, M.; Castoldi, A. F.; Chiusolo, A.; Colagiorgi, A.; Colas, M.; et al. Updated peer review of the pesticide risk assessment of the active substance metalaxyl-M (amendment of approval conditions). *EFSA J*. **2025,** *23*, e9573.
[10] Qamar, W.; Shahid, M. U.; Irfan, M.; Abbas, R. Z.; Faraz, A.; Hussain, R.; Alvi, M. A. Thiamethoxam toxicity: a review in one-health perspective. *Kafkas Univ. Vet. Fak. Derg*. **2023,** *29*, 557-570.
[11] Jatoi, A. S.; Hashmi, Z.; Adriyani, R.; Yuniarto, A.; Mazari, S. A.; Akhter, F.; Mubarak, N. M. Recent trends and future challenges of pesticide removal techniques–a comprehensive review. *J. Environ. Chem. Eng*. **2021,** *9*, 105571.
[12] Dolatabadi, M.; Naidu, H.; Ahmadzadeh, S. Adsorption characteristics in the removal of chlorpyrifos from groundwater using magnetic graphene oxide and carboxy methyl cellulose composite. *Sep. Purif. Technol*. **2022,** *300*, 121919.
[13] Tyagi, V.; Thakur, A. Applications of biodegradable carboxymethyl cellulose-based composites. *Results Mater*. **2023,** *20*, 100481.
[14] Izadi, M.; Bazli, L. Eco-friendly composites: developing sustainable solutions for modern engineering. *J. Compos. Comp*. **2025,** *7*, 1-9.
[15] Saad, S.; Elakremi, M.; Khiari, R.; Elaloui, E.; Salem, R. B.; Moussaoui, Y. Carboxymethylcellulose synthesis and advanced applications: A comparative analysis of posidonia oceanica and ziziphus lotus sources. In *Current Status and Opportunity in Fibre and Composites: Posidonia Oceanica*; Springer: Singapore, 2025; pp 83-104.
[16] Qiu, B.; Sun, T.; Li, M.; Chen, Y.; Zhou, S.; Liang, M.; Zou, H. High micromechanical interlocking graphene oxide/carboxymethyl cellulose composite architectures for enhancing the interface adhesion between carbon fiber and epoxy. *Compos. Part A Appl. Sci. Manuf*. **2020,** *139*, 106092.
[17] Pettignano, A.; Charlot, A.; Fleury, E. Carboxyl-functionalized derivatives of carboxymethyl cellulose: towards advanced biomedical applications. *Polym. Rev*. **2019,** *59*, 510-560.
[18] Thy, L. T. M.; Thuong, N. H.; Tu, T. H.; My, N. H. T.; Tuong, H. H. P.; Nam, H. M.; Phong, M. T.; Hieu, N. H. Fabrication and adsorption properties of magnetic graphene oxide nanocomposites for removal of arsenic (V) from water. *Adsorpt. Sci. Technol*. **2020,** *38*, 240-253.
[19] Bose, R.; Alanazi, A. K.; Bhowmik, S.; Garai, S.; Roy, M.; Pakhira, B.; Pramanik, T. Applications of graphene and graphene oxide as versatile sensors: a brief review. *Biointerf. Res. Appl. Chem*. **2023,** *13*, 457.
[20] Vallinayagam, S.; Rajendran, K.; Lakkaboyana, S. K.; Soontarapa, K.; Remya, R.; Sharma, V. K.; Kumar, V.; Venkateswarlu, K.; Koduru, J. R. Recent developments in magnetic nanoparticles and nano-composites for wastewater treatment. *J. Environ. Chem. Eng*. **2021,** *9*, 106553.
[21] Sirajudheen, P.; Nikitha, M. R.; Karthikeyan, P.; Meenakshi, S. Perceptive removal of toxic azo dyes from water using magnetic Fe_3O_4 reinforced graphene oxide–carboxymethyl cellulose recyclable composite: adsorption investigation of parametric studies and their mechanisms. *Surf. Interfaces* **2020,** *21*, 100648.
[22] Yu, H.; Hong, H.-J.; Kim, S. M.; Ko, H. C.; Jeong, H. S. Mechanically enhanced graphene oxide/carboxymethyl cellulose nanofibril composite fiber as a scalable adsorbent for heavy metal removal. *Carbohydr. Polym*. **2020,** *240*,

116348.
[23] Hummers, J.; William, S.; Offeman, R. E. Preparation of graphitic oxide. *J. Am Chem. Soci*. **1958,** *80*, 1339-1339.
[24] Min, H. S. Scanning electron microscopy analysis of thin films: a review. *Res. Asp. Chem. Mat. Sci*. **2022,** *5*, 16-28.
[25] Mibielli, R. B. I.; Gerber, T.; Mazzarino, L.; Veleirinho, M. B.; Yunes, R. A.; Maraschin, M. Development of a spectrophotometric method for quantification of carvacrol in nanoemulsions. *Rev. Bras. Farmacogn*. **2021,** *31*, 116-120.
[26] Vomocil, J. A. Porosity. In *Methods of Soil Analysis: Part 1 Physical and Mineralogical Properties, Including Statistics of Measurement and Sampling*; American Society of Agronomy, Inc.: American, 1965; pp 299-314.
[27] Badawy, M. E. I.; Taha, M. A. I.; Abdel-Razik, R. K.; Abo-El-Saad, M. M. Preparation, characterization, and pesticide adsorption capacity of chitosan-magnetic graphene oxide nanoparticles with toxicological studies. *Environ. Sci. Poll. Res*. **2025,** *32*, 5159-5185.
[28] Bauer, T.; Blachar, G.; Greenfeld, B. E. Rank-stability of polynomial equations. *Int. Math. Res. Not*. **2025,** *2025*, rnaf173.
[29] Taha, M. A. I.; Badawy, M. E. I.; Abdel-Razik, R. K.; Younis, H. M.; Abo-El-Saad, M. M. Mitochondrial dysfunction and oxidative stress in liver of male albino rats after exposing to sub-chronic intoxication of chlorpyrifos, cypermethrin, and imidacloprid. *Pestic. Biochem. Physiol*. **2021,** *178*, 104938.
[30] IBM Corp. *IBM SPSS Statistics for Windows, Version 25.0*; IBM Corp.: Armonk, NY, 2017.
[31] Apandi, N. M.; Zailani, W. W. A.; Izwan, K. N. K.; Zakaria, M.; Zulkarnain, N. N. Graphene oxide as carbon-based materials: a review of geopolymer with addition of graphene oxide towards sustainable construction materials. *Construct. Build. Mat*. **2024,** *411*, 134410.
[32] Rostamiiranagh, A.; Mohammad-Rezaei, R. Magnetic graphene oxide functionalized dimercaptosuccinic acid/putrescine as a selective and stable solid-phase extraction adsorbent for preconcentration and speciation of arsenic (III) in water samples. *Int. J. Environ. Anal. Chem*. **2025,** *105*, 2569-2586.
[33] Sadighian, S.; Bayat, N.; Najaflou, S.; Kermanian, M.; Hamidi, M. Preparation of graphene oxide/Fe_3O_4 nanocomposite as a potential magnetic nanocarrier and MRI contrast agent. *ChemistrySelect* **2021,** *6*, 2862-2868.
[34] Huang, Z.-M.; Liu, X.-Y.; Wu, W.-G.; Li, Y.-Q.; Wang, H. Highly elastic and conductive graphene/carboxymethylcellulose aerogels for flexible strain-sensing materials. *J. Mater. Sci*. **2017,** *52*, 12540-12552.
[35] Mohamood, N. F. A.-Z. T.; Halim, A. H. A.; Zainuddin, N. Carboxymethyl cellulose hydrogel from biomass waste of oil palm empty fruit bunch using calcium chloride as crosslinking agent. *Polymers* **2021,** *13*, 4056.
[36] Tungadi, R. The effect of ultrasonication time on particle size, polydispersity index and stability evaluation of anthocyanin liposomes. *Univers. J. Pharm. Res*. **2024,** *9*, 8-13.
[37] Serrano-Lotina, A.; Portela, R.; Baeza, P.; Alcolea-Rodriguez, V.; Villarroel, M.; Ávila, P. Zeta potential as a tool for functional materials development. *Catal. Today* **2023,** *423*, 113862.
[38] Rajora, A.; Nagpal, K. Suspensions: theory, formulation considerations, flocculated and deflocculated suspensions, and evaluation of suspension stability. In *Advances in Pharmaceutical Product Development*; Springer: Singapore, 2025; pp 199-218.
[39] Ahmad, S.; Ayoub, M. H.; Khan, A. M.; Waseem, A.; Yasir, M.; Khan, M. S.; Bajwa, T. M.; Shaikh, A. J. Diverse comparative studies for preferential binding of graphene oxide and transition metal oxide nanoparticles. *Colloids Surf., A* **2022,** *647*, 129057.
[40] Yu, H.; Wang, B.; Zhou, S.; Zhu, M.; Chen, W.; Chen, H.; Li, X.; Liang, S.; Wang, M.; Zheng, L. Polyvinylpyrrolidone functionalization induces deformable structure of graphene oxide nanosheets for lung-targeting delivery. *Nano Today* **2021,** *38*, 101151.
[41] Eltaweil, A. S.; Elgarhy, G. S.; El-Subruiti, G. M.; Omer, A. M. Carboxymethyl cellulose/carboxylated graphene oxide composite microbeads for efficient adsorption of cationic methylene blue dye. *Int. J. Biol. Macromol*. **2020,** *154*, 307-318.
[42] Bryan, M. Y. K.; Chai, P. V.; Law, J. Y.; Mahmoudi, E. Graphene oxide-chitosan composite material as adsorbent in removing methylene blue dye from synthetic wastewater. *Mat. Today: Proc*. **2022,** *64*, 1587-1596.
[43] Ibrahim, A. A.; Adel, A. M.; Abd El-Wahab, Z. H.; Al-Shemy, M. T. Utilization of carboxymethyl cellulose based on bean hulls as chelating agent. Synthesis, characterization and biological activity. *Carbohydr. Polym*. **2011,** *83*, 94-115.
[44] Mousavi, S. M.; Babapoor, A.; Hashemi, S. A.; Medi, B. Adsorption and removal characterization of nitrobenzene by graphene oxide coated by polythiophene nanoparticles. *Phys. Chem. Res*. **2020,** *8*, 225-240.
[45] Shakil, M. S. R.; Aktar, M. S.; Hossain, M. A.; Ahmed, S. Synthesis and application of carboxymethyl cellulose-graphene oxide composite for the mitigation of Pb^{2+} and Cd^{2+} from aqueous solution. *Clean Eng. Technol*. **2024,**

18, 100724.
[46] Mathew, J. T.; Shaba, E. Y.; Otori, A. A.; Inobeme, A.; Monday, M.; Adetunji, C. O.; Azeh, Y.; Jumai, M. J.; Bini, E. M.; Tanko, M. S.; et al. Use of activated carbons in pesticide removal from wastewater: review and future prospects. In *Pesticide Removal Methods from Wastewater: Proactive Approaches and Future Trends*; Pathak, P. D., Jadhav, A. R., Deokar, S. K., Patil, S., Eds.; Apple Academic Press: New York, 2025; pp 89-132.
[47] Pratap Singh Raman, A.; Thakur, G.; Pandey, G.; Kumari, K.; Singh, P. An updated review on functionalized graphene as sensitive materials in sensing of pesticides. *Chem. Biodivers*. **2024,** *21*, e202302080.
[48] Khawaja, H.; Zahir, E.; Asghar, M. A.; Rafique, K.; Asghar, M. A. Synthesis and application of covalently grafted magnetic graphene oxide carboxymethyl cellulose nanocomposite for the removal of atrazine from an aqueous phase. *J. Macromol. Sci., Part B* **2021,** *60*, 1025-1044.
[49] Ighalo, J. O.; Yap, P.-S.; Iwuozor, K. O.; Aniagor, C. O.; Liu, T.; Dulta, K.; Iwuchukwu, F. U.; Rangabhashiyam, S. Adsorption of persistent organic pollutants (POPs) from the aqueous environment by nano-adsorbents: a review. *Environ. Res*. **2022,** *212*, 113123.
[50] Kamari, A.; Ngah, W. W. Isotherm, kinetic and thermodynamic studies of lead and copper uptake by H_2SO_4 modified chitosan. *Colloids Surf. B Biointerfaces* **2009,** *73*, 257-266.
[51] Qi, C.; Zhao, L.; Lin, Y.; Wu, D. Graphene oxide/chitosan sponge as a novel filtering material for the removal of dye from water. *J. Colloid Interface Sci*. **2018,** *517*, 18-27.
[52] Araújo, C. S. T.; Almeida, I. L. S.; Rezende, H. C.; Marcionilio, S. M. L. O.; Léon, J. J. L.; De Matos, T. N. Elucidation of mechanism involved in adsorption of Pb (II) onto lobeira fruit (*Solanum lycocarpum*) using Langmuir, Freundlich and Temkin isotherms. *Microchem. J*. **2018,** *137*, 348-354.